Assessment of the water mass dynamics over the western Mediterranean in the MEDRYS1V2 reanalysis

Quentin-Boris Barral[1], Bruno Zakardjian[1], Franck Dumas[2,3], Pierre Garreau[3], Jonathan Beuvier[4]

[1] Université de Toulon, Aix-Marseille Université, CNRS, IRD, MIO, Toulon, France

[2] SHOM, Service Hydrologique et Océanographique de la Marine, 13 rue de Chatelier, CS592803, 29228 Brest CEDEX2, France

[3] IFREMER, UNIV. Brest, CNRS UMR 6523, IRD, Laboratoire d'Océanographie Physique et Spatiale (LOPS), IUEM, 29280, Plouzané, France

[4] CNRM, Météo-France/CNRS, 42 avenue Gaspard Coriolis, 31057 Toulouse Cedex 1, France

Key points

We study the water masses dynamics of the western Mediterranean from a 20yr reanalysis using a θ-S based algorithm of water masses fraction.

The method allows detecting anomalous events of deep water creation/descruction likely due to the assimilation process.

Results highligth the impact of deep water formation on the surface and intermediate regional circulation.

Abstract

We present an assessment of the water mass dynamics in a reanalysis of the Mediterranean Sea with a focus on the Western basin. We use a θ-S based algorithm to compute the fractions of the main western Mediterranean water masses : Atlantic and modified Atlantic Waters (AW, mAW), Western and Levantine Intermediate Waters (WIW and LIW)and Western Mediterranean Deep Waters (WDW). The reanalysis retains the known mean characteristics of the water masses, their seasonal to interannual variability and main circulation patterns when compared with the literature. The imprints of winter mixing is particularly obvious with coherent variations of water mass volumes, mainly the yearly creation of WIW from mAW on northernmost shelves and of WMDW from all surface and intermediate layers during years of deep water formation. The results also highlight some unrealistic events of variability of the WMDW volume that are likely due to the data assimilation process. Re-computing the water mass volumes and transports without these altered years allowed to highlight the possible disruption of the large-scale barotropic cyclonic circulation in the Eastern Algerian basin in response to major DWF events over the Gulf of Lion. The reanalysis also shows an overtopping of WMDW in the Sardinia Channel in 2009 leading to a major backward flow of mAW from the Tyrrhenian to the Algero-Provençal basin. Both processes affects the circulations of AW and mAW over the whole western Mediterranean.

Plain Language Summary

Defined as the large-scale oceanic circulation driven by surface heat and freshwater fluxes, the oceanic thermohaline circulation is a major player in the Earth's climate, as it distributes excess heat and carbon dioxide due to human activities into the deeper layers of the ocean over the long term. The Mediterranean Sea is unique in that it has its own thermohaline circulation due to its semi-enclosed configuration, a climate-driven water deficit (~ 1 m/year) balanced by a net inflow of Atlantic waters, and significant heat loss in winter leading to the formation of intermediate and bottom water masses. This thermohaline circulation has a time scale of around 100 years, 10 times less than the global circulation, and has been shown to respond rapidly to the Northern Hemisphere climate variability. We have used a 20-year ocean reanalysis, i.e. a system that combines model and observations, to characterize and quantify the circulation of water masses in the western Mediterranean, from seasonal to interannual scales. Our study reveals that the main weakness of reanalysis lies in deep-water dynamics, whereas it has a marked imprint on surface and intermediate circulations. Understanding of the Mediterranean's future requires a better representation of its deep dynamics.

Abbreviations

Water Masses : AW for Atlantic Water; LIW for Levantine Intermediate Water; mAW : for modified Atlantic Water; mIW for mixed Intermediate Water; TDWfor Tyrrhenian Deep Water; TIW for Tyrrhenian Intermediate Water; WIW for Western Intermediate Water; WMDW for Western Mediterranean Deep Water

Currents : AC for Algerian Current; AE for Algerian Eddy; BC for Balearic Current; ECC for East Corsican Current; NC for Northern Current; SE for Sardinian Eddy; WCC for West Corsican Current

Others : DWF for Deep Water Formation; EMT for Eastern Mediterranean Transient; MEDRYS for MEDiterranean ReanalYSis; MLD for Mixed Layer Depth; SLA for Sea Level Anomaly; WMT for Western Mediterranean Transition

1. Introduction

The Mediterranean Sea has the unique particularity of having its own and well defined thermo-haline circulation, almost independent from the global one. This is due to its particular configuration : a semi-enclosed sea suffering a dry, windy and relatively warm regional climate that makes it a concentration basin where evaporation exceeds precipitation and run-offs (Nof, 1979; Béthoux, 1980). This climate driven deficit of water (~0.5-1.0 m/year) is balanced by a net inflow through the Strait of Gibraltar between in-flowing AW and deeper out-flowing salty Mediterranean water (Nof, 1979; Millot, 1987; Béthoux & Gentili, 1999; Mariotti et al., 2002; Pellet et al., 2019). The incoming AW flows cyclonically in all the Mediterranean sub-basins toward the easternmost Levantine Basin and is continuously modified all along its path by mixing with saltier resident waters and air-sea exchanges. Simultaneously, severe heat loss and evaporation due to harsh atmospheric conditions in autumn and winter over the northern parts of the Mediterranean Sea causes convection to intermediate and deep layers (the deep water formation, DWF) in several areas and so to the recurrent formation of different intermediate and deep water masses. Those areas are mainly the Gulf of Lion for Western Mediterranean Deep

Water (WMDW), the Adriatic Sea and the Aegean Sea for the Easter Mediterranean Deep Water (EMDW) and in the northern Levantine Basin for the very salty Levantine Intermediate Water (LIW). All those locally produced water masses mix and spread all together with the AW to set up and maintain the Mediterranean ThermoHaline Circulation (MTHC, Robinson & Golnaraghi, 1994; Bergamasco & Malanotte-Rizzoli, 2010; Waldman et al., 2018; Pinardi et al., 2019). The MTHC has a time scale of about 100 years (10 times less that the global Ocean one) and has been shown to quickly respond to Northern Hemisphere climate variability, be it during the last glacial period (Cacho et al., 2000, 2001; Incarbona et al., 2016; Cortina-Guerra et al., 2021) or more recently in the early 90's when an abrupt shift in the intermediate and deep part of the eastern MTHC, called the Eastern Mediterranean Transient (EMT), has affected the water masses in both parts of the Mediterranean for at least a decade (Roether et al., 2007; Bergamasco & Malanotte-Rizzoli, 2010; Cardin et al., 2015; Li & Tanhua, 2020; Sisma-Ventura et al., 2021). Subsequent to the propagation of the EMT signal in the western Mediterranean and after a lack of intermediate and deep convection in the early 00's, the sudden return of DWF events in 2005 and after has led to a cooling and freshening of the intermediate waters associated with a warming and salting of the deep waters called the Western Mediterranean Transition (WMT, Lopez-Jurado et al., 2005; Schroeder et al., 2006, 2010, 2016; Pineiro et al., 2019, 2021; Amitai et al., 2021).

All climate models predict in the Mediterranean an increase in rainfall variability and strong warming and drying (Somot et al., 2008; de Sherbinin et al., 2014; IPCC AR6 WGI Full Report, 2021) while there is some evidence that the western DWF may collapse by mid-century due to increased stratification (Somot et al., 2006; Herrmann et al., 2008; Parras-Berrocal et al., 2021). Indeed, recent studies have shown the Mediterranean waters to have warmed at a rate four times larger than the global Ocean over the last decades (~0.04°C/year vs ~0.01°C/year, Bethoux et al., 1998; Vargas-Yanez et al., 2008; Nykjaer, 2009; Bensoussan et al., 2019; Pisano et al., 2020), affecting all layers throughout the Mediterranean. These warning signals have led, over the last twenty years or so, to an unprecedented effort of sampling, modeling and analysis. However, an integrated and quantitative view of the MTHC able to improve the monitoring and future predictions of climate-induced changes still remains a challenge (CIESM 2002; Theocharis, 2008; Somot et al., 2008; Fox-Kemper et al., 2019). Here, we focus on the western Mediterranean which is known to be a four-layer system (surface, winter subsurface, intermediate and deep waters, Juza et al., 2015) and has six main water masses which are commonly and clearly identified in the literature : the AW and mAW in near surface layers (0-200m), the Western Intermediate Water (WIW, ~200m) and LIW at intermediate depths (300-600m), the Tyrrhenian Deep Water (TDW, 500-1500m) and the WMDW at greater depths down to the bottom (Wust, 1961; Millot, 1987; Manzella & La Violette, 1990; Pinot et al., 1995; Millot & Taupier-Letage, 2005; Juza et al., 2013, 2019).

The AW incoming from the strait of Gibraltar (0.6-1.0 Sv, Soto-Navarro et al., 2010; Peliz et al., 2013; Skliris et al., 2018) is the first input of the western MTHC and, except the Rhône and Ebro rivers plumes, is the lightest and freshest water of the western Mediterranean (S~36.0 at the Strait of Gibraltar). It flows along the North-African coast within the Algerian Current (AC, Fig. 1), being spread and partially mixed northward in the Algerian basin by the Algerian Eddies (AEs, e.g. Millot, 1990; Puillat et al., 2002; Testor et al., 2005b; Escudier et al., 2016) before flowing eastward toward the Tyrrhenian and through the strait of Sicily towards the Eastern Mediterranean (Béranger et al., 2004; Jebri et al., 2016). MAW or mAW, for modified Atlantic Water is an acronym commonly used by many authors to designate the saltier AW due to its

ageing in the Mediterranean (e.g. Theocharis et al., 1993; Millot, 1999; Onken & Sellschopp, 2001; Puillat et al., 2002; Hassoun et al., 2015). It is sometimes also called old AW, (typical) Mediterranean Water or Mediterranean Surface Water, (Millot et al. 2006; Millot, 2007, 2009). Some others consider both the AW and mAW as a single entity (e.g. CIESM 2001, Millot & Taupier-Letage, 2005; Béranger et al., 2005; Millot, 2013; Fedele et al., 2022). Both the AW and mAW are restricted to the upper (0-200 m) layers but significantly differ in terms of salinity values, the latter reaching two salinity units greater values (~38.2-38.4) for the saltier ones in the Tyrrhenian and Ligurian Seas; hence the use of the appelation mAW for the present work. The saltier mAW from the Tyrrhenian fuels the East Corsican Current (ECC) and joins with the West Corsican Current (WCC) to feed the Northern Current (NC) that flows from the Ligurian to the Balearic Sea (Fig. 1).

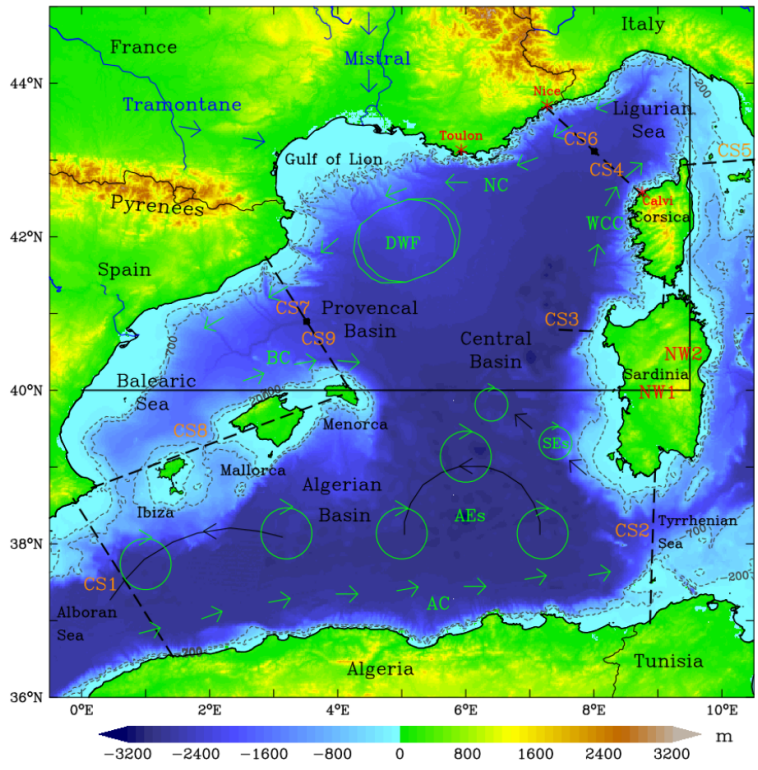

Fig. 1. Map of the western Mediterranean bathymetry and major circulations features. AC, BC, NC and WCC denote respectively the Algerian, Balearic, Northern and West Corsican currents. Large and small arrow circles denote the Algerian and Sardinian Eddies, respectively (AEs & SEs) while black arrows represent their paths. The oval shape locates the Deep Water Formation area. The CS sections locate where the transports of Table 2 have been calculated. The NW1 section locates the section of Fig. 3, and with NW2, both define the NWMED domain as in Somot et al. (2018). Bathymetry data are from etopo1.nc (NOAA National Geophysical Data Center. 2009)

The Levantine Intermediate Water (LIW) is the second major input of the western MHTC. LIW is produced in the Eastern Mediterranean by intermediate (~200-600 meters) convection in winter and is the saltier (S>39) of the Mediterranean (Millot, 2013; Ozer et al., 2017; Kubin et al., 2019). The LIW flows cyclonically along the continental slope at intermediate depths (200-600 meters) throughout the whole eastern basin and partly passes the strait of Sicily (Millot, 2013; Ben Ismail et al., 2014) to enter the western basin. When LIW enters the Tyrrhenian Sea, it mixes with resident deep waters (mostly WMDW) and forms the TDW (Astraldi & Gasparini, 1994; Sparnocchia et al., 1999; Gasparini et al., 2005), but still keeping a pronounced salinity signature (S>38.8 between 300-600 meters). Both the LIW and TDW follow a counterclockwise circulation in the Tyrrhenian (Falco et al., 2016; de la Vara et al., 2019; Iacono et al., 2021) before they leave through the Sardinia Channel to enter the Algero-Provençal basin where it flow northwestward along the western coasts of Sardinia and Corsica or are spreaded out westward in the central basin by the Sardinian Eddies (SEs) (Rhein et al., 1999; Testor et al., 2005a; Bosse et al., 2015; Send & Testor, 2017).

The WIW is a winter cooled mAW due to cold and dry winds (Mistral and Tramontane) blowing over the shelf of the Gulf of Lion (GoL), the Provençal basin and the Ligurian Sea. Although not originally the saltiest of the mAW (~38.3), its cooling is sufficient to increase its potential density so as to make it sit between the warmer mAW and the deeper LIW at an intermediate depth of about 200-300 meters. It flows then mostly along the continental slope across the Balearic Sea and later through the Ibiza and Mallorca channels down to the Alboran Sea (Salat & Font, 1987; Puig et al., 2013; Juza et al., 2019; Vargas-Yanez et al., 2012, 2020). Stronger winter wind forcing over the GoL and the Provençal basin regularly causes vertical convection through the WIW and LIW/TDW that can reach the seafloor in some years, leading then to the renewal of the WMDW (MEDOC group, 1970; Millot, 1999; Schroeder et al., 2008ab; Waldmann et al., 2016, 2017ab; Testor et al., 2018, Keller Jr. et al., 2022). Intermediate convection during less severe winters produces a slightly less dense water that stands and stacks between the LIW and older deep water with thermohaline characteristics similar to the TDW. Constrained by the southward increasing bathymetry, the denser WMDW (σ_θ>29.10 kg m^{-3}) then spreads mostly southward across the whole Algero-Provençal basin up till the Alboran Sea. The WMDWs can sometimes pass through the Sardinia channel to enter the Tyrrhenian when exceptional DWF uplifts the older and lighter WMDW up to the strait sill, as following the WMT (e.g., Beuvier et al., 2012; Schroeder et al., 2016; Li & Tanhua, 2020).

To better understand the dynamics of these water masses, it is necessary to be able to follow their behavior and interactions, their entry or exit, their propagation and their mixing through the numerous mesoscale to sub-mesoscale eddies that are found throughout the NW Mediterranean. This challenge is hardly achievable with at-sea observations alone, while numerical modeling may not be free of biases and unrealistic trends due to uncertainties in forcing, initial conditions

and unresolved sub-grid processes. By combining, thanks to data assimilation systems, modeling and observations in a coherent physical framework, ocean reanalysis offers a good compromise, particularly for multi-decanal series which allow us to approach the climatology of the system and its inter-annual variability (Balsameda et al., 2015; Aznar et al., 2016). However, the reanalysis has its own weaknesses, mainly due to the assimilation process which, by forcing the model trajectory to converge towards independent observations, does not guarantee the pure conservation of heat and salt and can therefore alter the characteristics of the water masses.

This work is based on a reanalysis of the Mediterranean Sea, called MEDRYS1V2 (Hamon et al., 2016; Beuvier et al., 2016), with two main objectives : first, to assess the mean characteristics and distribution of water masses over the western Mediterranean as produced by the reanalysis, and second, to gain insight, characterize and quantify the circulation of these different water masses from seasonal to inter-annual time scales. We built a simple and efficient method to detect the water masses in the western Mediterranean and track their circulation and mixing over the twenty-year reanalysis (Section 2.2). The results are first analyzed using the mean thermohaline characteristics of each water mass to assess the robustness of the reanalysis in terms of water mass conservation. Climatological average of water mass volumes and transports are then assessed based on known circulation patterns (Section 3.1). In a second step, we analyze the time series of specific properties and volumes of each water mass (Section 3.2). In a third step, we focus the analysis on the DWF impact on surface dynamics at the climatological scale and by reference to the WMT (Section 3.3). We discuss the algorithm and the results, and conclude in Section 4.

2. Data & Methods

2.1. The MEDRYS1V2 Reanalysis

The study is based on the MEDRYS1V2 reanalysis which begins in October 1992 and ends in June 2013 with daily outputs (Hamon et al., 2016; Beuvier et al., 2016). These two decades allow us to compute quite good climatology of water mass volumes and transports and to observe several different episodes. MEDRYS1V2 is a configuration of the NEMO-MED12 model (which has a spatial resolution of 1/12° and 75 z levels sharpened near the surface) that uses the SAM2 assimilation scheme (Lellouche et al., 2013). The simulation is forced by the atmospheric ALDERA dataset (Hamon et al. 2016), a downscaling of the ERA-Interim reanalysis (Dee et al., 2011) with the ALADIN-Climate regional climate model (Colin et al., (2010) for the description of the version 5 of ALADIN-Climate used to produce the ALDERA dataset). Satellite SST, altimetry and *in situ* temperature-salinity (θ-S) profiles are assimilated. SST data was assimilated at a resolution of 1° and comes from NOAA 1/4° gridded radiometer products (Reynolds et al., 2007) without trusting any observation within 50 km off the coasts. The along-track Sea Level Anomaly (SLA) AVISO product (1992-2013) is assimilated one every three points and combined with the Mediterranean MDT from Rio et al. (2011). Assimilated *in situ* θ-S profiles from the CORA4 database (Cabanes et al., 2013) uses only one profile within 0.1° per day per platform. The reanalysis is initialized end of September 1992 with the state of a twin free run (same model configuration as MEDRYS1V2 but without data assimilation), which starts in October 1979. It takes about 9 months after its start for the reanalysis to achieve its spin up (see Hamon et al., 2016). Following results and validation hence do not take into account the first three seasons of the reanalysis (autumn 1992 to spring 1993).

2.2. The Detection Algorithm of Water Masses

Among the oldest tools of physical oceanography, the θ-S diagram is classically used to analyze the mixing and distribution of water masses. It is based on the fact that the mixing of two water masses builds a straight line, allowing hence to determine the fraction of those for all sampled depth along this mixing line. The method is only a little more complicated for the mixing of three water masses considering that the sum of their fraction must equal unity. It becomes intractable for four water masses or more without considering at least another one conservative variable (e.g. Manca et al., 2006; Schroeder et al., 2008b; de Brauwere et al., 2007). Even in these cases, the other used variables should have to be sampled with the same spatio-temporal resolution that the θ-S data, which is a hard to achieve task. Other methods can be found in the recent literature, such as clustering based methods (e.g. Kim et al., 1991; Cardin et Celio., 1997; Zhu et al., 2019) sometimes combined with EOF analysis on vertical profile of temperature and salinity (e.g. Hjelmervik & Hjelmervik, 2013; Bauch & Cherniavskaia, 2018; Gao et al., 2020), but were not considered given their high computing cost over a 20-y reanalysis.

Indeed, we rather use the fact that, with the exception of transitory convection events, the vertical distributions of the different water masses are constrained by their relative buoyancy, i.e. are vertically ordered with increasing potential density. The water mass sorting algorithm was so-defined from the climatological (i.e. 20-y average) θ-S diagram computed from the reanalysis (Fig. 2) assuming that, over the western Mediterranean, the water column can be partitioned in three main layers, each with different θ-S mixing trends. AW and mAW ($37<S<38.45$, $\theta>13{,}5°C$) are above 200-300m and can be easily distinguished from salinity alone. Temperature ranges seasonally from 13°C to more than 25°C in this upper layer and may only help in winter to identify WIW as cooled mAW ($\theta<13.5°C$). Below 300m depth, a second mixing line reveals the transition toward a salinity maximum that marks the LIW core. Below this salinity maximum, the θ-S diagram shows a third and almost linear mixing line from LIW to the WMDW, including TDW-like mixed intermediate waters. The water masses' sorting algorithm hence uses at first a partitioning of the water column based on potential density and, in a second step, ad hoc salinity and temperature dilution ratios along the three previously identified mixing lines. Using potential density based functions rather than fixed depths allows to dynamically adjust this partitioning of the water column all along the reanalysis. Likewise, dilution ratios are used afterward rather than net truncations that do not resolve water mass mixing and may generate spurious discontinuity effects in the vicinity of the threshold values used to discriminate the water masses. The main algorithm's hypotheses are as follows (computations' steps and equations are detailed in Appendix A).

At first, the partition of the water column is made with two functions defining the surface (f_{surf}) and deep (f_{deep}) waters assuming the LIW marks the boundary between both (Appendix A.1). The surface layer is defined as all waters above the $\sigma_\theta(mAW)=28.964$ kg m^{-3} isopycnical ($f_{surf}=1$), assumed to mark the lower bound of the mAW core, and considering below a linear decrease of f_{surf} toward zero between $\sigma_\theta(mAW)$ and $\sigma_\theta(LIW) = 29.061$ kg m^{-3}. The mAW's salinity (38.45) used to define $\sigma_\theta(mAW)$ is the maximum of time averaged sea surface salinity in the reanalysis (Fig. 2) and in observations in the Ligurian Sea (Marty & Chiavérini, 2010; Prieur et al., 2020). It is also the salinity minimum of WMDW (e.g., Puig et al., 2013; Houpert et al., 2016). The value used for $\sigma_\theta(LIW)$ is that of the original LIW in the eastern basin (taking $S=39$ and $\theta=15°C$) that is globally conserved in the reanalysis along the path of the LIW spreading (Fig. 2). The deep layer function is defined similarly assuming a linear increase from zero to

unity between LIW and WMDW, with a deeper bound σ_θ(WMDW) of 29.11 kg m^{-3} (assuming S=38.45 and θ=12.82°C) which is an often used lower bound for the WMDWs (e.g., Waldman et al., 2017ab; Somot et al., 2018; Testor et al., 2018). This function directly gives the fraction of WMDW (f_{WMDW}) in the algorithm.

The LIW is first tagged using a salinity dilution ratio between 38.45 and 39 (Appendix A.2). Note that as such, the LIW fraction (f_{LIW}) is the residual of the original LIW being previously mixed all along its path from the Levantine basin to the western basin. The AW is hence tagged (f_{AW}) using a salinity dilution ratio from S=36.0, i.e. the minimum salinity of inflowing AW through the Strait of Gibraltar (see Table 1), to S=38.45, i.e. the maximum of time averaged sea surface salinity in the reanalysis, coherently with the documented maximum value in the Ligurian Sea (Prieur et al., 2020). In addition, we included a patch below S = 36.0 to discriminate fresh water (f_{fresh}) of rivers, mainly the Rhône and Ebro Rivers, from the AW. This freshwater fix produces false AW detections in the region of freshwater influence of both rivers, where freshwater from both rivers would rather mix with resident mAW. However these false AW detections are of very limited extent due to the sharpness of the salinity fronts on the edges of the freshwater plumes and did not significantly affect volumes and transports estimates made later on.

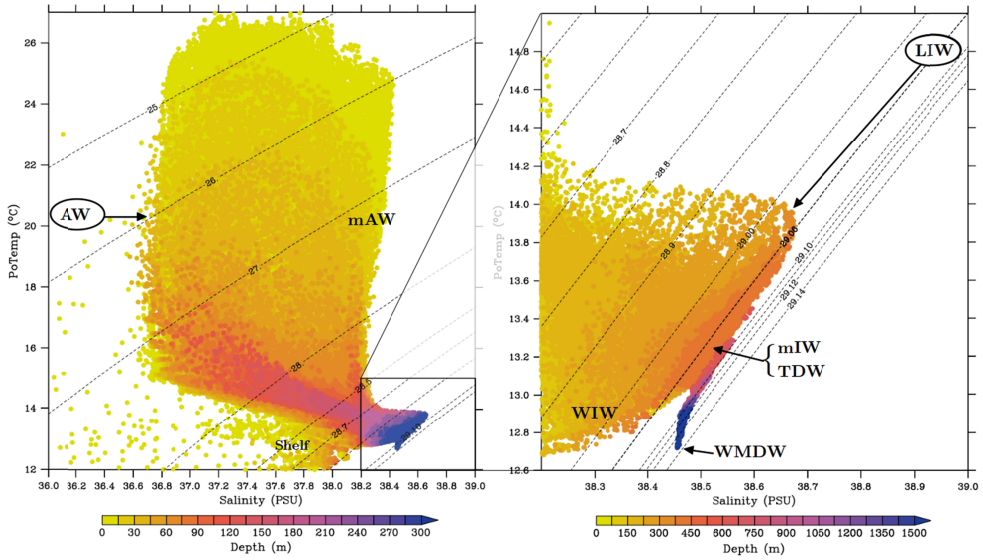

Fig. 2. θ-S diagram colored by depth of the full average of the 20-years MEDRYS1V2 reanalysis, illustrating the several known water masses in the western Mediterranean basin (except the Alboran and Tyrrhenian Seas' sub-basins as in Fig. 1). AW, mAW, WIW, LIW, mIW, TDW, and WMDW denote respectively Atlantic Water, modified Atlantic Water, Western Intermediate Water, Levantine Intermediate Water, mixed Intermediate Water, Tyrrhenian Deep Water, and Western Mediterranean Deep Water. Shelf locates Gulf of Lion's shelf water.

The mAW fraction (f_{mAW}) is then defined as the complementary of AW, freshwater and LIW

flags in the upper layer, i.e. $f_{mAW} = f_{surf} . [1 – (f_{fresh}+f_{AW}+f_{LIW})]$, with, in addition, a sub-partitioning of mAW to discriminate WIW using a temperature dilution ratio between 13°C and 13.5°C when θ is lower than 13.5°C (Appendix A.3). This WIW labeling is an intermediate method between a fixed range detection and the geometry-based method of Juza et al. (2019). At last, we define a pool of intermediate mixed waters, called mIW, as the complementary of the sum of all previously computed flags, i.e. $f_{mIW} = 1- (f_{fresh}+f_{AW}+f_{mAW}+f_{WIW}+f_{LIW}+f_{WMDW})$, that may include TDW as well as all partially mixed waters of similar thermohaline characteristics produced during intermediate or uncomplete DWF events over the GoL. None of those intermediate water masses is able to generate an inflection point on the θ-S diagram that may help to unambiguously discriminate them.

Fig. 3 shows an illustrative example of the θ-S-flags diagrams and corresponding vertical distribution of the so-tagged water masses for a zonal section at 40°N in the late-spring of 2009. Higher flag values properly match the known θ-S ranges of each water mass, mixing trends between each and vertical distributions. Waters above σ_θ=29.0 kg m^{-3} are mainly AW and mAW, showing a zonal transition between the Balearic Sea, where mAW are mostly found, and the central area where the signature of AW is slightly more pronounced. Both are tagged in the upper 300 m and well above the LIW. WIW is located between mAW and LIW and preferentially in the Balearic Sea in a vein of low temperature (13-13.3°C) and moderate salinity (38.1 to 38.4). LIW is tagged between 200 and 800m depth, preferentially on the Sardinian coast, but also showing some traces at great depths (2000-2200 m) likely resulting from a previous to 2009 convection event (Pineiro et al., 2021). The WMDW is labeled at depth (f_{WMDW} greater than 75% below 800m) and mainly below the 29.10 kg m^{-3} isopycnical. The mIW is tagged on the WIW/LIW and LIW/WMDW mixing lines, centered around the 29.06 kg m^{-3} isopycnical with a larger extent at depth (800 m).

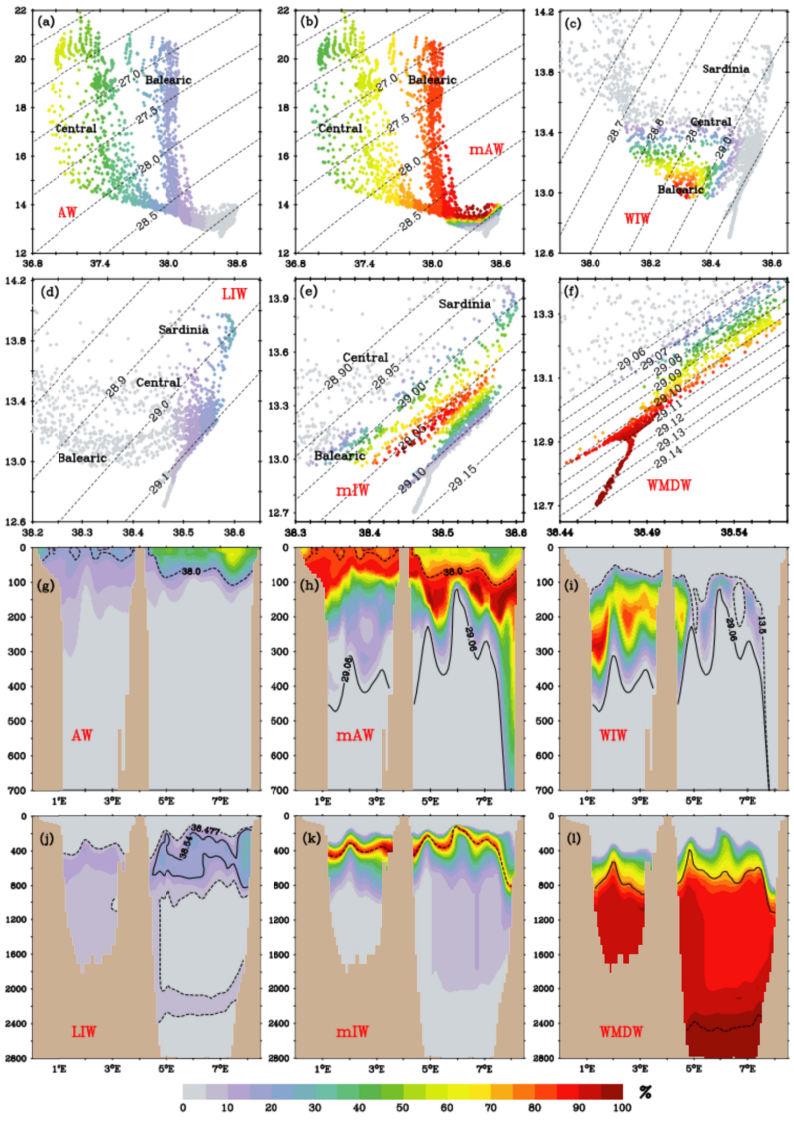
(a)
Balearic
Central
AW
(b)
Balearic
Central
mAW
(c)
Sardinia
Central
Balearic
WIW
(d)
LIW
Sardinia
Central
Balearic
(e)
Sardinia
Central
Balearic
mIW
(f)
WMDW
(g)
AW
(h)
mAW
(i)
WIW
(j)
LIW
(k)
mIW
(l)
WMDW
%

Fig. 3. θ-S diagrams (a-f) and (g-l) corresponding vertical cross-sections of the water mass ratios (%) along 40°N (NW1 section on Fig. 1) for 28 May 2009. Some critical isolines are shown on vertical section panels as : dotted line for the 38.00 isohaline (g-h); solid line for the 29.06 kg m^{-3} isopycnal (h) ; dotted line for the 13.5 °C isoherm and solid line for he 29.06 kg m^{-3} isopycnal (i) ; solid and dotted lines for the 38.54 and 38.477 isohalines, respectively (j) ; dotted line for the 29.06 kg m^{-3} isopycnal (k) ; solid line and dotted lines for the the 29.10 kg m^{-3} and 29.13 kg m^{-3} isopycnals (l), respectively. Balearic, Central and Sardinia locate the data of the Balearic Sea, the Central basin and the shelf's slope of Sardinia.

With the water masses marked in this way, several diagnostic quantities were calculated (see Appendix B for details of the calculations), first to check the robustness and efficiency of the algorithm over all the reanalysis, and second to extract the distributions and transports of each water mass. Based on the fact that the sum of the water mass fractions is always constrained to unity, these are first used as weighting factors to extract the volume-averaged thermohaline characteristics of each water mass over the study area. The core characteristics of each water mass are calculated similarly but using only the local maximum within the water column of the corresponding flag. We also calculated the depth range occupied by each water mass by averaging the minimum and maximum depths of each water column where the corresponding fraction is greater than 0.05 (5%). Still based on a sum of fractions equal to unity, the water mass fractions are then used to partition the volumes and advective fluxes for each grid cell, allowing the calculation of water mass-specific volumes and transports from the water column level (by depth integration) to the regional scale (by meridional and zonal integration).

3. Results

3.1. Average Thermohaline Characteristics, Volumes and Circulations of the Water Masses

This section presents climatological averages (i.e. 20-year averages) of the thermohaline characteristics, volumes and transports of each water mass as labeled by the algorithm. The average characteristics (θ, S, σ_θ, z) are first given in Table 1 for comparison with known literature values (references therein the table). The calculated specific volumes and transports are presented in Figure 4. Reported per square meter for each model grid point, the estimated volumes (in m^3) also correspond to the thickness of the water mass layer (in meters). Table 2 gives transport values computed at selected sections (see Fig. 1) to facilitate the comparisons with known transports of the major currents in the literature.

The mean salinity of the AW is estimated to be 37.565 ± 0.071 (average ± one standard deviation), slightly lower but more variable within the core of the water mass computed with the maximum flag value (37.289 ± 0.123). These values are about 1.5 units higher than those of the AW entering through the Strait of Gibraltar (S~36) and reflect the progressive mixing with the Mediterranean saltier waters in the Alboran gyre system and further east in the AC instabilities and associated AEs. The AW mean temperature is ca 15.954 ± 1.32°C, close to the mean values for the inflowing AW, with a standard deviation of 1.32-1.85 °C (core and whole estimates, respectively) that accounts for the seasonal cycle of surface layers in the area. As such, the AW is the lightest water mass, showing average potential density values less than 28.0 kg m^{-3}, a maximum depth of 135 ± 16 m and a core's mean depth close to the surface (22 ± 9 m).

371 **Table 1.** Historical and computed (20y and spatial average, standard deviation in brackets) values of
372 potential temperature, salinity, potential density anomaly and depth location of the water masses in the
373 western Mediterranean. The locations of historical studies are indicated with Lig., Bal, Prov., Lev, Alg.-
374 Prov and Tyr. denoting respectively the the Ligurian and Balearic Seas, the Provençal area, Levantine,
375 Algero-Provençal basin and Tyrrhenian Sea.

376

Water Mass		θ (°C)	PSAL	σ_θ (kg.m^{-3})	Depth range (m)	Location & period	References
AW		>15	36.0-36.4	<27	<200	Gibraltar, 1955-2007	Bryden et al., 1994; Millot, 2007, 2009; Carracedo et al., 2014
		14-25	37.5-37.8	~25	0-150	Bal. Sea & Alg.-Pro. 1996-2020	Vargas-Yanez et al., 2020; Barral et al., 2021; Fedele et al., 2022
	Full	15.954 (1.32)	37.565 (0.071)	27.702 (0.338)	min 0 (0) ave 34 (2) max 135 (16)	Alg.-Pro. 1993-2013	This study
	Core	16.907 (1.849)	37.289 (0.123)	27.273 (0.507)	ave 22 (9)		
mAW		>13	38.0-38.5	27.5-29	0-300	Lig. Sea & Prov. area 1980-2018	Marty & Chiaverini, 2010; Puig et al., 2013; Prieur et al., 2020
	Full	14.508 (0.605)	38.107 (0.04)	28.462 (0.147)	min 0 (0) ave 63 (8)max 253 (36)	Alg.-Pro. 1993-2013	This study
	Core	13.798 (0.355)	38.302 (0.042)	28.779 (0.09)	ave 114 (27)		
WIW		11.5-13.5	37.7-38.6	28.9-29.1	100-300	Bal & Pro 1983-2019	Salat & Font, 1987; Puig et al., 2013; Juza et al., 2019; Vargas-Yanez et al., 2012, 2020
	Full	13.204 (0.084)	38.356 (0.05)	28.953 (0.024)	min 131 (29) ave 151 (51) max 257 (33)	Alg.-Pro. 1993-2013	This study
	Core	13.217 (0.074)	38.358 (0.038)	28.953 (0.016)	ave 164 (32)		
LIW		≥15	39-39.2	29.06	200-500	Lev. basin1978-2017	Millot, 2013; Ozer et al., 2017; Kubin et al., 2019
		13.1-13.9	38.5-38.7	29.05-29.1	200-800	Alg.-Pro. 2000-2019	Puillat et al., 2006; Bosse et al., 2015; Mallil et al., 2021; Fedele et al., 2022
	Full	13.151 (0.046)	38.518 (0.009)	29.09 (0.009)	min 273 (28) ave 703 (96) max 1269 (401)	Alg.-Pro. 1993-2013	This study
	Core	13.385 (0.053)	38.564 (0.017)	29.077 (0.011)	ave 425 (40)		
TDW		12.8-13.7	38.43-38.7	>29.09	>700	Tyr. Sea1987-2018	Fuda et al., 2002; Buffett et al., 2017; Napolitano et al., 2019; Li & Tanhua, 2020
		>12.86	38.46-38.56		600-1900	Alg.-Pro. 1997-2002	Rhein et al., 1999; Send & Testor, 2017; Ben Ismail et al., 2021
mIW	**Full**	13.149 (0.086)	38.497 (0.018)	29.075 (0.006)	min 205 (26) ave 525 (138) max 1344 (402)	Alg.-Pro. 1993-2013	This study
	Core	13.309 (0.054)	38.518 (0.014)	29.057 (0.001)	ave 325 (51)		
WMDW		12.7-13	38.4-38.5	>29.1	>1500	Alg.-Pro. 1990-2014	Millot, 1999; Fuda et al., 2000; Puig et al., 2013; Schroeder et al., 2006, 2016; Knoll et al., 2017
	Full	12.910 (0.032)	38.476 (0.013)	29.108 (0.007)	min 360 (56) ave 1382 (85) max 2246 (21)	Alg.-Pro. 1993-2013	This study
	Core	12.783 (0.026)	38.461 (0.010)	29.122 (0.009)	ave 2192 (129)		

377

378 The AW is mainly detected (Fig. 4a) in the Algerian basin, within the AC and the AEs spreading

area toward 40-41°N with some intrusions in the Balearic Sea through the Ibiza Channel (see Millot, 1987; Pinot et al., 1995). The AW transport exiting the Alboran Sea is estimated to 0.58 ± 0.31 Sv (CS1 in Table 2), from which a little part passes the channel of Ibiza (0.08 ± 0.15 Sv, CS8) while the largest part flows eastward through the Sardinia Channel toward the Tyrrhenian (0.37 ± 0.25 Sv, CS2). In both cases, the standard deviations reflect a high variability (0.15-0.25 Sv) likely due to the mesoscale activity that prevails in the AC and AEs. There is no significant AW transport north to 41°N, i.e. only very low values (lower than 2×10^{-3} Sv) due to traces of tagged AW (f_{AW} under 5%), left by the use of a linear salinity dilution ratio between AW and mAW in the algorithm rather than a fixed threshold. The imbalance in AW transport between the inflow from Alboran and the outflow through the Sardinia Channel is compensated by a significant eastward flow of mAW through the Sardinia Channel (see below), highlighting the mixing of AW with the resident Mediterranean waters in the instabilities of the AC and the AEs.

The labeled mAWs show higher mean salinities of 38.107 in the whole and 38.302 in the core, but in both cases with a low standard deviation (ca 0.04). The mean temperatures are lower than for the AWs (13.798°C and 14.508°C for the core and the whole, respectively), and less variable (standard deviation less than 0.355-0.605°C), mainly due to their more northerly and deeper distribution (see Fig. 3). Mean densities are therefore higher (28.462-28.779 kg m^{-3}), as are the whole's maximum (253 ± 36 m) or the core's mean (114 ± 27 m) depths. The algorithm labels an eastward, increasing volume of mAW in the Algerian basin in response to the salinity increase along the path of AW toward the Tyrrhenian and, coherently, a higher volume of mAW in the Tyrrhenian. While the transports through the Sardinia Channel show both eastward and westward flows for the mAW, the net balance is eastward (0.35 ± 0.47 Sv) and compensates for the imbalance of AW transport between the Alboran exit and the Sardinia Channel. In the northern part of the basin (North of 40°N), the mAW is tagged along the shelf's slope, showing the well-known cyclonic circulation from the West Sardinia to the Balearic Sea with an offshore undulating return flow between Mallorca to Sardinia around 40°N. The lower amount of mAW in the center of this gyre is consistent with the well-known isopycnal doming in the wintertime convective areas (e.g., Prieur et al., 2020). The mean transport of mAW increases from 0.12 ± 0.36 Sv along the shelf's slope of West Sardinia (CS3), to 0.49 ± 0.41 Sv in the WCC off Calvi (CS4). Then, being reinforced by the ECC from the Tyrrhenian (+0.29 ± 0.31 Sv, CS5), the mAW flow finally reaches 0.72 ± 0.43 Sv in the NC off Nice (CS6), but clearly decreases off the Gulf of Lion before entering the Balearic Sea (0.32 ± 0.50 Sv, CS7). Part of this decrease comes from the long-time average effect of winter times when mAW temporarily vanishes due to their conversion in new WIW during the coldest months and ultimately in WMDW during deep convection events.

The average thermohaline characteristics of WIW are close to those of mAW, showing only a slightly higher salinity (38.356 ± 0.05) and, as expected, a lower temperature (13.204 ± 0.084 °C) with no significant difference between the full and core estimates. The low standard deviations of the mean temperatures of the WIWs are due to the narrow range of temperatures that defines them and their short period of contact with the ocean-atmosphere interface. The WIW is generally defined as colder than 13°C, but the 20-y average uses all days of the year and not only winter days when the recent WIW is at its coldest. In addition, Juza et al. (2019) and Vargas-Yanez et al. (2020) have shown a warming trend in the WIW of 0.5°C over the last decade. The corresponding mean potential density of the WIW (28.953 kg m^{-3}) is slightly higher than that of the mAW's core (28.779 kg m^{-3}), leading to a depth range (131 ± 29 to 257 ± 33 m) that lies between the mAW and LIW cores (114 and 425 m). The average total volume of WIW

over the Algero-Provençal domain is 17.3 $\times 10^3$ km^3 , distributed mainly along the Gulf of Lion shelf-slope and over most of the catalano-balearic area in agreement with estimates of Juza et al. (2013, 2019). The WIW average transport off the Catalan coast is estimated to be 0.20 ± 0.32 Sv, part of which escapes from the Balearic Sea through the BC (0.11 ± 0.17 Sv) and a lesser amount through the channels of Ibiza and Mallorca toward the Alboran Sea (0.08 ± 0.12 Sv). These estimates are consistent with those of Juza et al. (2013), although they use a much higher resolution model (1/40°) and a shorter period. Finally, as the algorithm considers WIW as cold mAW, WIWs' volume and transport mirror the decrease of mAW ones from the Gulf of Lion to the Balearic Sea. Adding both transports compensates for the loss of mAW between Nice and the Balearic Sea.

Table 2. Twenty year averaged water masses transports (Sv) and standard deviations (in brackets) computed across the transects shown Fig. 1. The ones for the Alboran Sea and the Sardinia Channel are positive eastward ; all others are positive northward. Transports between Corsica and Sardinia are not shown (lower than 10^{-5} Sv).

	AW	mAW	WIW	LIW	mIW	WMDW
CS1: Alboran Sea	0.579 (*0.306*)	0.133 (*0.342*)	-0.086 (*0.088*)	-0.060 (*0.050*)	-0.324 (*0.226*)	-0.198 (*0.576*)
CS2: South of Sardinia	0.373 (0.254)	0.345 (0.472)	0.0 (0.01)	-0.194 (0.160)	-0.088 (0.148)	-0.065 (0.462)
CS3: WCC off Sardinia	0.018 (0.062)	0.171 (0.368)	0.0 (0.062)	-0.009 (0.112)	-0.136 (0.405)	-0.246 (0.748)
CS4: WCC off Calvi	0.062 (0.048)	0.487 (0.412)	0.09 (0.141)	0.056 (0.159)	0.348 (0.892)	0.142 (0.408)
CS5: East of Corsica	0.034 (0.044)	0.294 (0.312)	0.006 (0.037)	0.010 (0.015)	0.005 (0.014)	0.000 (0.001)
CS6: NC off Nice	-0.075 (0.05)	-0.72 (0.43)	-0.142 (0.219)	-0.068 (0.165)	-0.351 (0.890)	-0.163 (0.401)
CS7: NC off Pyrenees	-0.044 (0.093)	-0.323 (0.497)	-0.204 (0.325)	-0.047 (0.082)	-0.295 (0.372)	-0.387 (0.842)
CS8: Balearic channels	0.082 (0.154)	-0.025 (0.351)	-0.083 (0.115)	-0.011 (0.023)	-0.139 (0.206)	-0.063 (0.154)
CS9: BC off Menorca	0.095 (0.101)	0.310 (0.377)	0.111 (0.170)	0.027 (0.077)	0.143 (0.337)	0.374 (0.858)

The algorithm gives the LIW mean salinity as 38.518 ± 0.009, with only a slightly higher value for the core (38.564 ± 0.017). These low values are consistent with a -0.4 PSU loss due to the LIW dilution from the Levantine to the Western basin (e.g. Millot et al., 2013; Schroeder et al., 2020). Its relatively low mean temperatures (13.151 °C) can be interpreted in the same way, while less marked within the warmer LIW core (13.385 °C). Note that the estimated global LIW characteristics also include the older LIW which is distributed over all depths, especially during deep convection events, leading to traces of LIW in the deeper layers (see Fig. 3). This bias also affects the calculated depth range (273 ± 28m to 1269 ± 401m) and overall potential density (29.09 kg m^{-3}). However, the core calculation better matches the main LIW vein flowing along western Sardinia at about 400 meters depth in Bosse et al. (2015), with salinities over 38.56, temperatures over 13.39 °C and a potential density of 29.075 kg m^{-3}. This latter value is slightly higher than the one used in the algorithm (29.06 kg m^{-3}) as a specific characteristic of the original LIW, but closer to the one usually found in the northwestern Mediterranean (e.g., Puig et al., 2013; Schroeder et al., 2020). The largest LIW volume is detected over the Sardinia Channel,

given the proximity of the Tyrrhenian where LIW is known to accumulate (e.g., Sammari et al., 1999). LIW volumes decrease rapidly westwards with lowest (or even null) volumes over the shallowest areas, i.e. the GoL shelf, the East of Corsica and the Balearic Islands, ensuring that the algorithm effectively identifies them as intermediate waters. The associated transports show a turbulent eddy-like propagation between southern Sardinia and the Balearic archipelago, and a weak cyclonic flow (0.01-0.07 Sv) along the shelf slope over most of the western basin, except for an offshore separation of the main flow (0.027 Sv) at the entrance to the Balearic Sea somewhat linked toward northern Corsica. This cyclonic flow along the shelf slope is consistent with historical finding about the LIW behavior (e.g. Millot & Taupier-Letage, 2005) and the eddy-like flow in the central area would reflect the average effect of the SEs' drift (e.g. Testor et al., 2005a; Bosse et al., 2015). The absence of a significant LIW flow along Corsica north of 41°N is coherent with the detachment of the "SUddies" northwest of Sardinia in Bosse et al. (2015) while the offshore LIW flow midway between Menorca and Corsica follows the mAW and WIW recirculations in the northern gyre has, to our knowledge, never been suggested nor demonstrated.

The mean density of the tagged WMDW is close to the usual definition value of 29.10 kg m^{-3}, both for the total (29.108 ± 0.007 kg m^{-3}) and the core estimates (29.122 ± 0.009 kg m^{-3}). The WMDW is detected at a depth greater than 360 ± 56m (fractions greater than 5%) with a maximum depth (2246 ± 21m) and a core depth (2192 ± 129m) that closely follows the average bottom depth of the area. Its density-based tagging gives mean salinities of 38.476 (entire) and 38.461 (core) with small standard deviations (0.010-0.013), close to the usually observed range (see Table 1). The mean temperatures are also close to the usual estimates, being 12.783 ± 0.032 and 12.910 ± 0.026 °C for the ensemble and core, respectively. Due to its greater vertical extent, the WMDW volumes are of a higher order than other water mass volumes, and closely follows the bathymetry of the basin, the higher values being in the southern deepest area. It could be surprising that the highest volume is not found in the DWF area, but this reflects the rapid (within a few months e.g. Beuvier et al., 2012) southward spreading of newly formed WMDWs following the general increase in bathymetry to the south. The WMDW transports reveal a turbulent eddy-like circulation between southern Sardinia and the Balearic Archipelago and two cyclonic circulations over, respectively, the south-western basin between the Balearic Archipelago and North Africa and the north-western Liguro-Provençal area. The associated transports (Fig. 4 and Table 2) are of the same order as those of mAW and mIW, the greater depth range of the WMDW (thousands of meters) compensating for the lower velocities (below 5 cm/s) that prevail in the deeper layers.

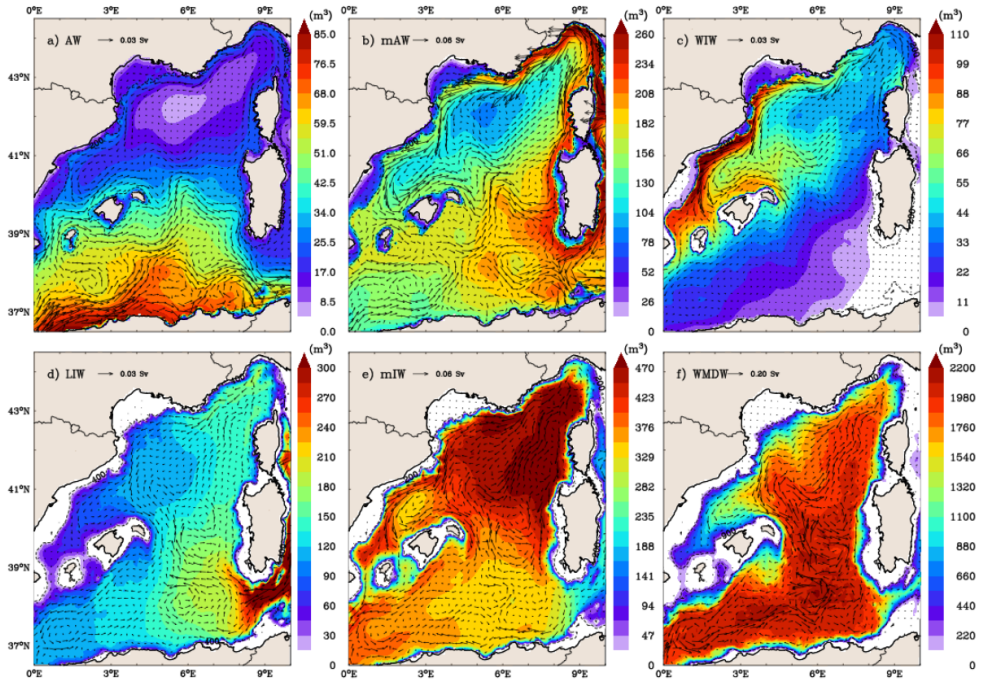

Fig. 4. Climatology of model grid water mass volumes (m^3) and transports (Sv) averaged over the 1993-2013 period: Atlantic Water (a), modified Atlantic Water (b), Western Intermediate Water (c), Levantine Intermediate Water (e), mixed Intermediate Water (e) and Western Mediterranean Deep Water (f). A scale arrow for transport values is shown on each panel.

As the mIW flag adds up what is left of all the other water masses, it is not a defined water mass but a residual mixture likely including TDW and more generally all intermediate waters from the eastern basin that may have passed the Sicily and Sardinia Channel (e.g. Millot et al., 2013, Schroeder et al., 2020), as well as those produced in the Northwestern provençal area due intermediate convection events. As such, its average characteristics cannot be objectively compared with the literature, but have to be coherent with the surrounding water masses. The mean salinities of the mIW (38.497 ± 0.018 for the whole and 38.518 ± 0.014 for the core) are midway between those of the LIW and the WMDW, thus well on the mixing line between them. In contrast, the mean temperatures (13.149 ± 0.086 and 13.309 ± 0.054) are slightly warmer than the average between LIW and WMDW which is more like 13 °C. The average potential density of the whole mIW is 29.075 kg m^{-3}, close to that of LIW, while that of the core is slightly lower at 29.057 kg m^{-3}. This reflects the fact that mIW is also labeled on a significant part of the upper intermediate layers, i.e. between the mAW/WIW and the LIW and not only in the deep layers below the LIW (see Fig. 3). The range of calculated mIW depths is consistent with these findings, showing a minimum of 205 ± 26 m, close to the maximum depths of the mAW and WIW, a core depth of 325 ± 50vm and a maximum depth of 1344 ± 402 m close to the LIW's one. The mIW volumes are the second highest, twice as high as mAW or WIW but five times

lower than WMDW, and have a general distribution opposite to WMDW with higher values in the most north-eastern part of the area. The circulation patterns are similar but less pronounced than those of the WMDW, except over the Balearic Sea where they rather follow those of the mAW/WIW. The corresponding transport values are most often intermediate between mAW and WIW over the northern part of the basin, ranging from 0.1-0.3 Sv (Table 2), but predominate through and south of the Balearic islands.

3.2. Time Series of Thermohaline Characteristics and Volumes of the Water Masses

Given the coherent long term mean of the water mass characteristics, volumes and circulations described in the previous section, we now look for their variability over the whole 20-y of the reanalysis. To do so, we present the time series of the characteristics (Fig. 5) and volumes (Fig. 6) of the water masses, with the corresponding maximum mixed layer depth (MLD) and DWF area extent (Fig. 6). The temperature variability on the surface water masses (AW, mAW) is first driven by the seasonal radiative cycles and enforced by strongest winds in winter time, i.e. classically, a cooling in autumn and winter and a warming in spring and summer. The mAW salinity shows a weaker (and even sometimes unclear) seasonal variability while the AW salinity does not show any seasonal cycles, coherently with the almost constant flow of AW through the strait of Gibraltar. This nearly constant AW flow also explains the low variability of the AW volume (Fig. 6). The seasonal variability of densities of the water masses then mainly depends on their temperature. By contrast, the mAW volumes exhibit a marked seasonal cycle with winter drops that mirror the increases of WIW volumes, materializing the conversion of mAW to WIW in winter time. Coherently, all WIWs' thermohaline characteristics show strong seasonal variations (Fig. 5c) with minimum temperature and salinity in winter (ca 13.0°C and 38.25) and increasing values from spring to summer due to its mixing with surrounding warmer water masses from below (the LIW) and from above (AW and mAW) given the summertime stratification of the surface layers. As such, the WIWs' volumes range from 10×10^3 km^3 in summer to 28×10^3 km^3 in winter close to the range estimated by Juza et al. (2019) for 2011-2013 (10×10^3 - 50.10^3 km^3). Note that the most severe drops in mAW volumes, which exceed the increase in WIW, occur during the DWF years (e.g., 1999 and 2005), affecting as well the WIW thermohaline characteristics.

On longer time scales, the mAW and AW salinities' time series show periods of alternating increase and decrease, but of limited amplitude (0.15) and not concomitant in time. We also note that maxima of mAW's volume tend to increase during the periods with several years of low or no convection (1996-1998, 2001-2002, 2007-2009) and, conversely, stay nearly constant during periods of consecutive medium to strong convection (1999-2000, 2003-2006, 2010-2013). This suggests that the destruction of the mAW by DWF in the northern sub-basin is generally balanced later in the year by its production by mesoscale horizontal mixing in the AEs' while several consecutive years of low or no convection may favor the accumulation of mAW over the whole basin. However, there are some exceptions to this global rule in 2001-2002 (stagnating mAW maximum volume instead of an increase) and in 2009 (increasing summer's mAW maximum volume instead of a stagnation). In the first case, it seems that from summer to summer, the period of no or low convection was too short to significantly affect the mAW volume. The 2009 year is an exceptional case that will find a more rational explanation later (Section 3.3). Lastly, the AW volumes exhibit similar, but low, drops during years of medium to strong convection followed by relaxing periods during low or no convection years. This similarity between the AW and mAW pluri-annual variability is likely due to the use of a salinity

ratio in the algorithm that retains a small amount of AW over the northern part of the basin. As the years of medium to strong convection are more frequent during the second half of the reanalysis, this leads to a general tendency of decreasing AW amount (-25 %) over the whole area.

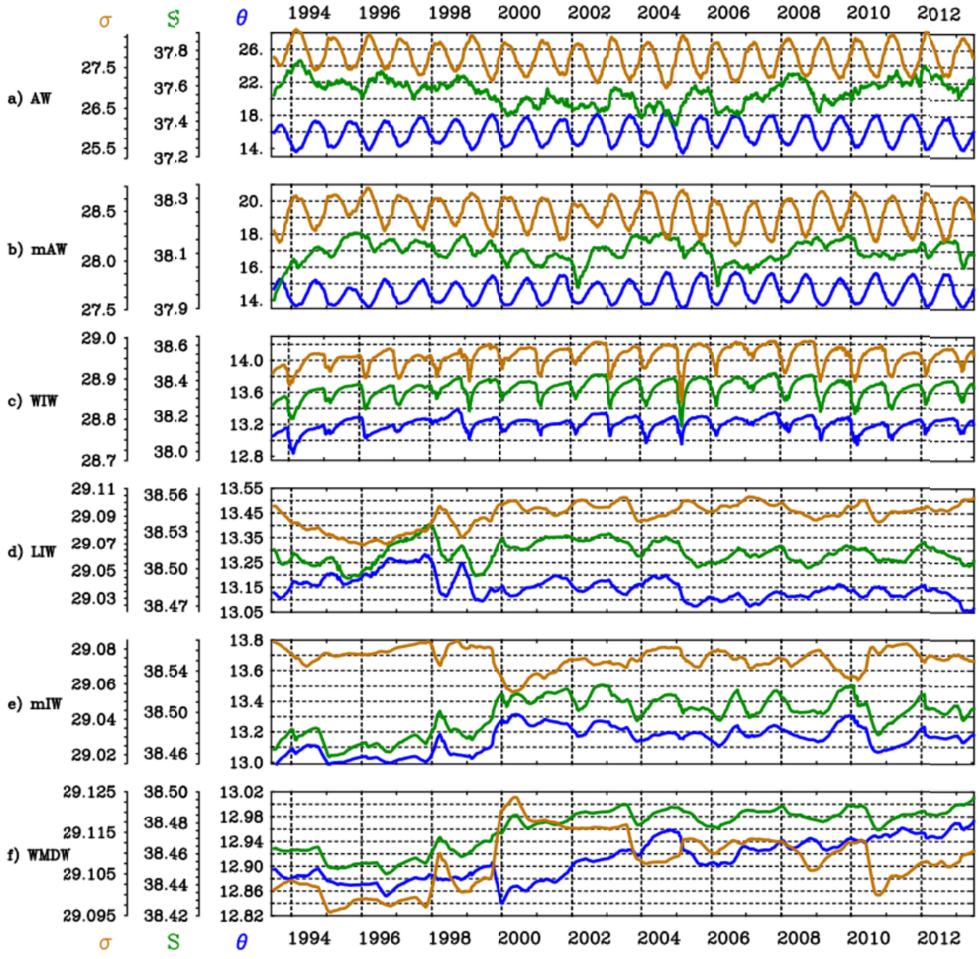

Fig. 5. Time series of average σ_θ (kg m^{-3}, brown lines), θ (°C, blue lines) and S (green lines) characteristics for the Atlantic Water (a), modified Atlantic Water (b), Western Intermediate Water (c), Levantine Intermediate Water (e), mixed Intermediate Water (e) and Western Mediterranean Deep Water (f).

In contrast, the characteristics and volumes of LIWs, mIWs and WMDWs do not vary seasonally, but rather show two different dynamics before and after the 1998-2000 period. The early years of the simulations show ambiguous thermohaline variations for LIWs, mainly a period of slow temperature increase (+0.15°C in 1993-1995), followed by an increase of both temperature and salinity peaking in late 1997, and alternating increases and decreases until the

end of 1999. At the same time, the LIW volume starts to slowly increase after 1995, more suddenly in 1999-2000 and again slowly until 2003 (Fig. 6d). It is constantly high later (about twice the initial volume of 30×10^3 km^3) but with still some interannual variations ($\pm 20 \times 10^3$ km^3). The thermohaline characteristics and volumes of mIW and WMDW are more stable during the first four years, but clearly evolve during 1998-2000 toward a higher salinity that remains for the rest of the reanalysis (+0.04 and +0.02, respectively) and an increased variability. Recalling that the reanalysis was initiated with results from a twin free run, a longer spin-up than the nine months initially considered (see section 2.1) could probably explain the questionable variability observed in the very early years of the reanalysis (1993-1994). The salinization of the middle and deep layers during 2000 was already noted by Hamon et al. (2016) in a previous version of the reanalysis (MEDRYS1V1). They attributed it to a biased volume correction term of the SLA model equivalent. This misfit tends to compensate for the SLA error by densifying the water columns. As the assimilation system is more constrained on temperature (due to better data coverage) than on salinity, this adjustment has a stronger effect on salinity, especially at depth due to the very low number of data assimilated below 600 meters depth before 2005. That being said, the increase in LIW volume in 1999-2000 does not coincide with the gradual salinization of LIW that starts earlier and drops off sharply in 1998. Rather, it coincides with an increase of the LIW flux through the Sardinia Channel (not shown), beginning in late 1998 and peaking (0.35 Sv) in late 1999 -early 2000. This increased LIW flux mainly comes from a slight increase of salinity (+0.04) of the LIW incoming from the Tyrrhenian, while velocities of the intermediate layers (200-600m) only show a very slight acceleration (+0.01 cm s^{-1}). This suggests that the accumulation of salt and LIW in the Algero-Provençal basin may also be related to the EMT that slowly propagated higher salt content toward the western Mediterranean from 1997 to 2004 (Schneider et al., 2014; Amitai et al., 2021). However, this statement must be qualified because the transport of LIW in the Channel of Sicily does not increase as much as in the Channel of Sardinia and remains almost constant (not shown). Both processes (i.e., a biased SLA adjustment or the westward EMT propagation) may have occurred simultaneously but would be difficult to distinguish since the biased SLA adjustment also affects the Eastern Mediterranean (see Hamon et al., 2016, Beuvier et al., 2016).

After 2000, WMDW and mIW show more stabilized behaviors with a variability that is mostly driven by the interannual variability of DWF, as evidenced by the conversion of mIW to WMDW (1999, 2005-2006, 2012-2013) and, conversely, a slow decrease (increase) in WMDW (mIW) volume during periods without DWF (2001-2002, 2007-2008). The effect of DWF is less pronounced on LIW volume, probably because the algorithm tends to retain the memory of the LIW salinity anomaly within the newly formed WMDW (see Fig. 3 for example). The WMDW volume is estimated to be about $600 \pm 100 \times 10^3$ km^3 for the entire area (0 to 10°E) and 270 ± 30 10^3 km^3 when calculated for the same NWMED area as in Somot et al. (2018) (see Fig. 1). This baseline of WMDW volume is a little higher than in Rixen et al. (2005) and Somot et al. (2018) (mean of 185×10^3 km^3 over 1980-2002), mainly due to the algorithm that uses a density fraction, rather than a fixed density threshold, but the increases in deep water volume during DWF events ranging about 50-180 $\times 10^3$ km^3 are in good agreement with Somot et al. (2018), Beuvier et al. (2012), Waldmann et al. (2016) and Testor et al. (2018).

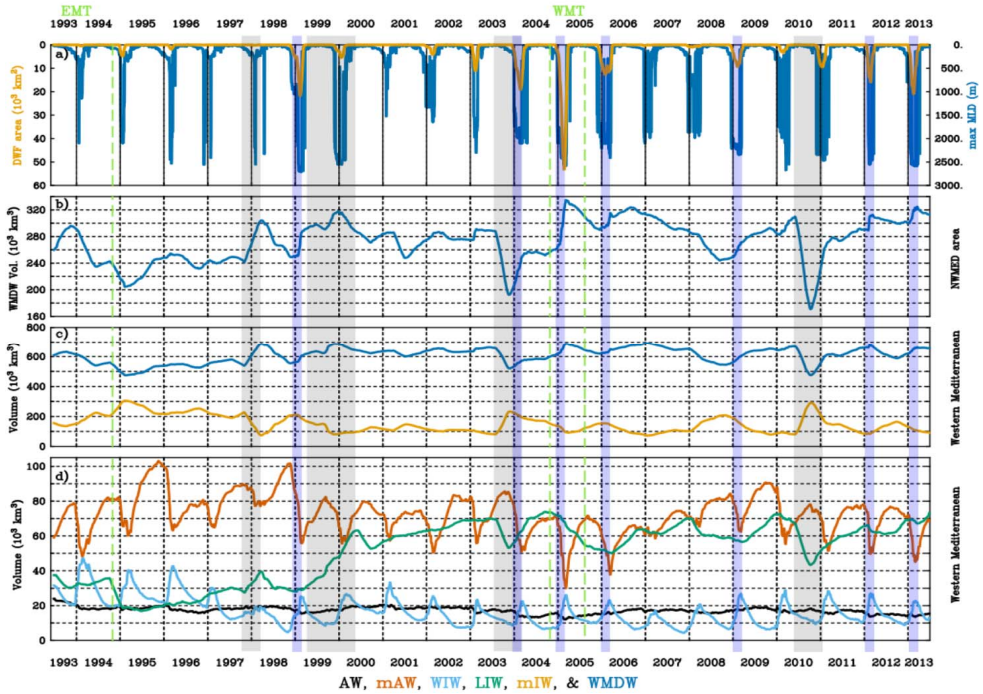

Fig. 6. Time series of the MLD maximum and extent of the DWF area over the NWMED (a) as Somot et al. (2018) (see Fig. 1) and volumes of WMDW in the NWMED area (b) and of all the water masses over the whole studied area (c, d, see bottom of the figure for the water masses color codes). The computations excludes the Alboran and Tyrrhenian Seas. Vertical gray rectangles locate the 1999 LIW accumulation, the 1998 dubious WMDW production event and the 2003 and 2010 events of WMDW destruction. Vertical blue rectangles locate the DWF periods. EMT and WMT denote Eastern Mediterranean Transient and Western Mediterranean Transition.

Conversely, some years make exceptions to this behavior, especially 2003 and 2010 showing high losses of the LIW (-25% and -40%) and WMDW (-20% and -25%) volumes mirrored by gains in mIW volume (about +150% and +250%). Likewise, the year 1998 inversely shows an increase (decrease) of the WMDW (mIW) volumes (+27%, -63%) while it is widely recognized that 1998 is not a DWF year (e.g. Somot et al., 2018). These dubious events of WMDW production (1998) and mixing or destruction (2003 and 2010) are detailed in Fig. 7. For 1998, the WMDW volume anomaly (by reference to the climatological one) suggests that the problem originates from the most southwestern area (likely in the Alboran Sea) and propagates northeastward on a large part of the basin (Fig. 7a). The associated transport anomalies show a considerably strengthened circulation (+2Sv) establishing a large anticyclonic gyre over the eastern Algerian basin, which is in contradiction with the well-known cyclonic gyre prevailing in this area (e.g., Send & Testor, 2017). Spatially averaged θ-S time series, over the southwestern area where the anomaly emerges, show that the WMDW volume anomaly mainly originates from a sudden increase of salinity (+0.02) near the bottom in December 1997 (Fig. 7dgj) that

reaches 1000 m in some months. It is followed by a cooling (-0.15 to -0.27 °C) of similar vertical extent. These thermohaline changes cause a drastic increase in density over a wide depth range with the 29.12 kg m^{-3} isopycnal reaching 600 m from mid-February to June 1998 (Fig. 7j), this being too shallow to be realistic in this region. Consequently, the algorithm diagnoses higher WMDW fractions, leading to dubious increased volumes. The years 2003 and 2010 are inverted situations with the WMDW volume anomalies showing WMDW destructions located over the whole Provençal basin (Fig. 7bc). The WMDW transport anomalies are not marked over the volume anomaly area, likely due to lowered WMDW fractions, but reach ca 1 Sv in numerous eddy-like structures over a large part of the Algerian basin. These anomalies are due to two similar events of desalination in the 600-2200 m range lasting several months. The drop in salinity reached -0.02 in the core (1800 m) of the anomaly in 2003 and -0.03 between 800 and 2000 m in 2010. There is no temperature changes in 2003, but an increase in 2010 that reached +0.08°C, strengthening the drop in potential density. In both cases, the isopycnals of 29.10 kg m^{-3} fall from 600 to 2000 m (Fig. 7kl), leading the algorithm to diagnose much lower WMDW fractions (less than 30%) and consequently lower volumes over a large part of the water column.

In all of these three cases, there is no physical process that can be invoked to explain such changes in the salinity and heat contents of deep and intermediate waters over such large areas. Those are more likely due to biases in the assimilation processes, either through subregional SLA adjustments or local vertical profiles adjustments, that can propagate over large areas. It is not in the scope of this study to clearly identify these biases or malfunctioning of the assimilation processes, but we note that the 1998 event just follow a short period of intensive CTD operations in the Alboran Sea during the ALMOFRONT-2 campaign (Prieur et al., 2003) while the availability of CTD profiles in the Mediterranean was generally low before the Argo era (i.e., before 2005) and limited to the 0-1000m range (Hamon et al. 2016). The sudden arrival of a higher level of information at depth in the assimilation system may have over-constrained the model. Likewise, the 2003 event just follows the 2003 heat wave that has been shown to markedly impact the SST over the northwestern Mediterranean and the circulation in the Central Mediterranean (Olita et al., 2007; García-Herrera et al., 2010). It is not unlikely that the model and/or the assimilation system may have poorly or differently handled the steric effect of this exceptional heat wave, leading to a destabilization of the assimilation system for the SLA. Note that WMDW volume calculations using a fixed threshold (such as 29.10 or 29.12 kg m^{-3}, Somot et al., 2018) yielded much more unrealistic estimates during these anomalous events, with stronger and more sudden variations (a few days, not shown). This indicates that the problem does not come from the water mass detection algorithm and rather supports the hypothesis of accidental biases in the assimilation system.

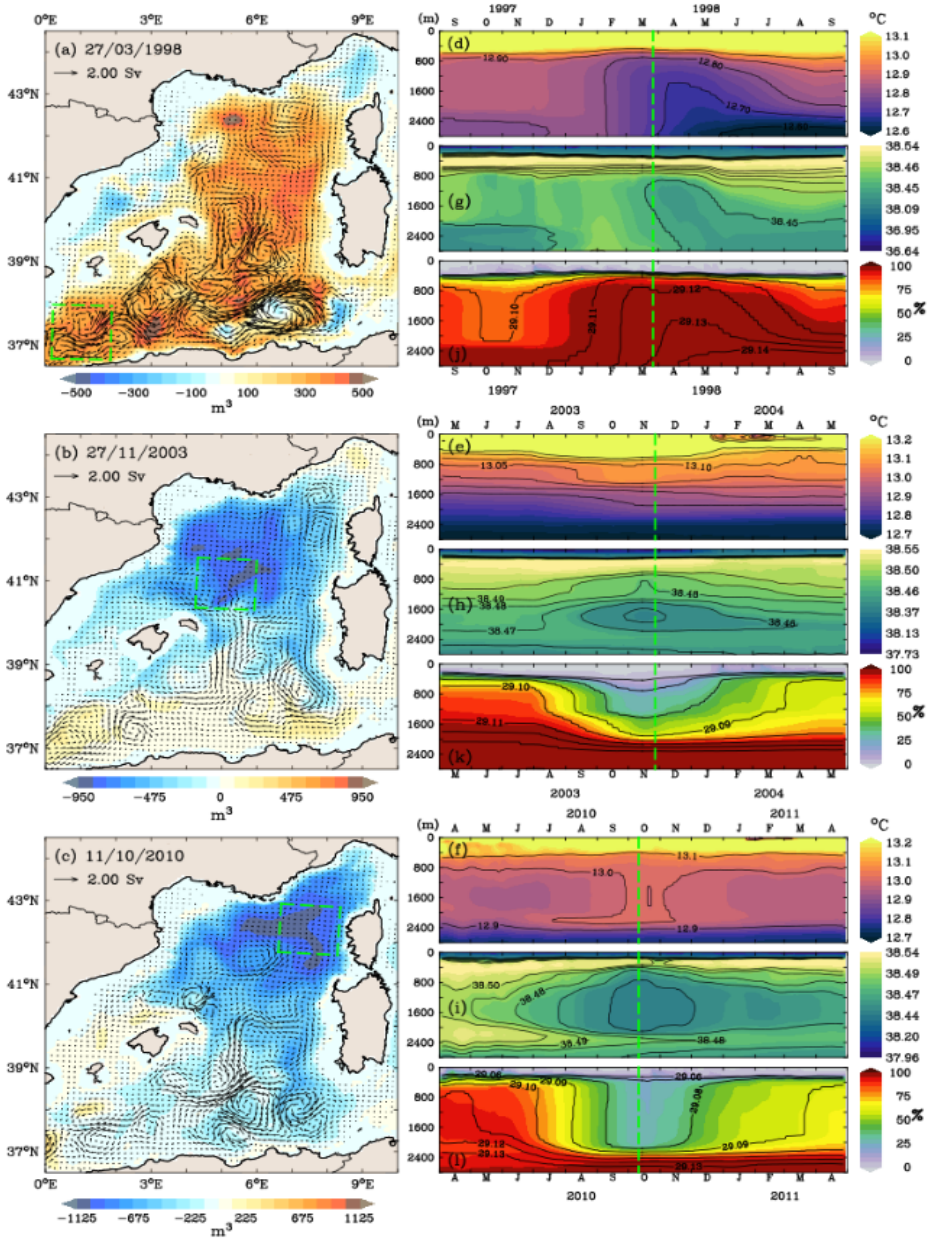
(a) 27/03/1998
2.00 Sv
(b) 27/11/2003
2.00 Sv
(c) 11/10/2010
2.00 Sv
0°E
3°E
6°E
9°E
43°N
41°N
39°N
37°N
−500 −300 −100 100 300 500
−950 −475 0 475 950
−1125 −675 −225 225 675 1125
m3
(m)
°C
1997
1998
2003
2004
2010
2011
(d)
(e)
(f)
(g)
(h)
(i)
(j)
(k)
(l)
12.90
12.80
12.70
13.05
13.10
13.0
12.9
38.45
38.48
38.47
38.50
38.49
38.46
29.12
29.13
29.14
29.10
29.11
29.09
29.08
29.06

Fig. 7. Anomalies of the WMDW volumes (by reference to the climatology of Fig. 4f) at the dates of maximum of the anomalous events of 1998 (a), 2003 (b) and 2010 (c), and corresponding year-long centered times series of spatially averaged temperature (d, e, f), salinity (g, h, i) and WMDW ratio (j, k, l) in the most impacted areas. The black arrows on the left panels show the WMDW transport anomalies. The green squares show the spatial domains used for averaging time series. The vertical green lines on right panels indicate the same day as on the left panels. Isopycnals (kg m^{-3}) are shown on the WMDW fractions' time series.

Beyond that, the reanalysis seems to resist these artifacts, which do not last more than a few months in terms of water mass volume (Fig. 6) and characteristics (Fig. 5). The impact in terms of deep water transport is more questionable, especially for the 1998 event for which the increase in WMDW transport over the Algerian basin and the inverted barotropic gyre lasted a few more than two years. We therefore recalculated the long-term mean volumes and transports for each water mass without the years 1998-1999, 2003, and 2010, as shown in Fig. 8. There are no significant differences in the volumes and transports of AW, mAW and WIW between Fig. 4 and Fig. 8 showing that the dubious events have had no effect on surface water masses. The new estimates for LIW, mIW and WMDW better highlight a deep cyclonic gyre in the eastern Algerian basin that is much more consistent with the literature (Testor et al., 2005b; Send & Testor, 2017). This mean cyclonic gyre was hidden by the strong anticyclonic gyre generated by the suspicious 1998 WMDW event, maintained until early 2000. The mIW and LIW also now exhibit this deep cyclonic circulation (Mallil et al., 2021), leading to cumulative transports of deep and intermediate water mass of about 2.5 ± 0.5Sv, only slightly lower than those reported by Send & Testor (2017) (4.0 ± 1.0Sv). For the six water masses, the largest volume differences from the first guess appear primarily in the western Algerian basin, consistent with the removal of the 1998 WMDW event, but do not exceed 10%.

3.3. Possible Connections of Deep and Surface Dynamics

The corrected climatology of water mass circulations (Fig. 4) highlights a deep gyre in the eastern Algerian basin in controlling the dynamics of deep and intermediate water masses. It has been suggested previously that this deep gyre may also control the surface path of AEs (Isern-Fontanet et al., 2006; Escudier et al., 2016; Pessini et al., 2018; Mallil et al., 2021). Although clearly an artifact, the 1998 WMDW production event in the Alboran Sea suggests that the deep gyre of the eastern Algerian basin may be highly sensitive to the arrival of newly formed deep water. In addition, Barral et al. (2021) showed that the DWF over the northern sub-basin can shift the northern boundary of the AWs, i.e. the Balearic-Sardinian frontal zone, one degree southward. They hypothesized that this would be due to a weakening in the formation and northward propagations of AEs during DWF years. To reexamine this hypothesis, we recomputed the mean water mass volumes and transports by separating the years with (2004-2006, 2009, 2011-2012, 6 years mean) and without DWF (1993-1997, 2000-2002, 2007-2008, 10 years mean) based on the maximum MLD and DWF area (Fig. 6a).

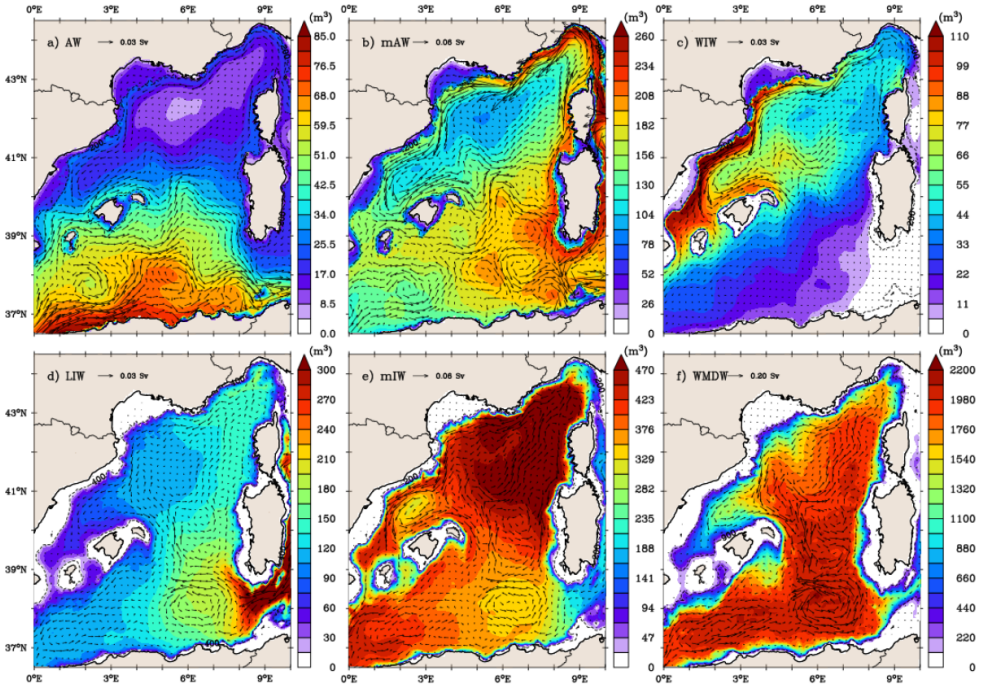

Fig. 8. Same as Fig. 4, without the years 1998-1999, 2003 and 2010.

For each water mass, the difference in mean volumes and transports between the two regimes are presented in Fig. 9. Years with DWF correctly show larger volumes of WMDW in the northwestern part of the basin, mainly in the known DWF area around 42°N-5°E, as well as increased transport of WMDW from the DWF area to northern Menorca and southward. The volume differences over the central Liguro-Provençal area for the mAW, WIW and mIW illustrate the conversion of surface and intermediate waters to WMDW when DWF occurs. The LIW volume is higher over the entire basin during DWF years in contradiction with the usual finding of its destruction during DWF events. This is partly due to the algorithm that retains memory of the LIW in deep layers after DWF events (see Sec. 3.1 and Fig. 3), but may also reflect the 1999 increase in LIW volume (Section 3.2), as all of the used DWF years occur after 2004. Furthermore, the differences in transport estimates show an acceleration of the along-slope cyclonic circulation over the Liguro-Provençal area for all surface and intermediate water masses. This acceleration of the regional cyclonic circulation has been suggested for a long time, based on heat and water budget (e.g., Bethoux et al., 1982; Astraldi & Gasparini, 1994) or dynamical considerations (e.g., Crépon & Boukthir, 1987; Madec et al., 1991) and clearly evidenced in dedicated modeling study (e.g., Hermann et al., 2008) but, to our knowledge, never on such climatological mean. Except for a thin area on the west coast of Corsica which will be discussed later, the water mass volumes over the northern along-slope circulation are not significantly affected, showing that the response is almost kinematic. Conversely, there are

significant changes in the AW volumes around and east of the Balearic Sea, showing that the shape of the northern (southern) extension of the AW (mAW) reservoir is modified toward less AW north of 39°N. This is consistent with our previous study that shows a DWF-induced meridional shift of the haline frontal zone that prevails between Menorca and Sardinia (Barral et al. 2021). This regime shift also largely affects the amount of mAW at the West of Sardinia and above the Algerian gyre, suggesting that less mAW may be produced by mixing in the AEs or to a lesser extent and activity of the AEs following a DWF event.

The difference in transports estimates between the two regimes also shows a marked inversion of the deep circulation in the area of the eastern deep Algerian gyre when DWF occurs, comforting the hypothesis of a disruption, or at least, a marked weakening of the barotropic gyre in response to the increased southward flow of the WMDW. Except WIW which is not detectable in this region, all the surface (AW, mAW) and intermediate (LIW, mIW) water masses show the same tendency. For LIW and mIW, this is likely due to the algorithm that maintains a link between the intermediate water masses and the WMDW through the use of salinity and potential density fractions, but it is also coherent with Send and Testor (2017). The alignment between the circulations of surface (AW, mAW) and deep water masses over the eastern deep Algerian gyre is less intuitive, but not so surprising if this long term mean is seen as retaining the long-term average of the paths of the AEs as guided by the deep barotropic gyre (Isern-Fontanet et al., 2006; Escudier et al., 2016; Pessini et al., 2018; Mallil et al., 2021). The weakening of the deep eastern Algerian gyre would induce a lesser northern extent of the AEs, as suggested above regarding the differences in AW and mAW volumes, hence a weakened signature of their paths on the surface circulation.

Surprisingly, it is not 2005, the most convective year in the time series (Fig. 6a, Schroeder et al. 2008a; Somot et al., 2018), that have the largest effect on the annual circulations of surface and intermediate water masses, but the year 2009 with an overflow of WMDW towards the Tyrrhenian that induced a strong return current of mAWs at the surface. This 2009 event is clearly visible on the upper panel of Fig. 10 which shows the water mass fluxes through the Sardinia Channel. The transports of WMDW and mAW differ from the rest of the time series, from mid-2008 to the end of 2009, both in intensity (larger than 1Sv) and sign, and are almost perfectly opposite. This overflow of the WMDW onto the sill in 2009 has been previously documented (Schroeder et al., 2016) and is attributed to the deposition on the seafloor in 2005 of the newly formed WMDWs, followed by several moderate DWF events in 2006, 2008 and in 2009. Each of these DWF events results in successive WMDW deposition, year after year, with the top of accumulated WMDW reaching 1900 m in 2009, the depth of Sardinia Channel sill (e.g. Schroeder et al., 2016; Li and Tanhua, 2020; Ben Ismail et al., 2021). The two transport anomalies peak late-June 2009, 4 months after the 2009 DWF events, a time scale for WMDW propagation that is consistent with Schroeder et al (2008a) and Beuvier et al (2012).

Formatted: Font: (Default) Times New Roman, Pattern: Clear

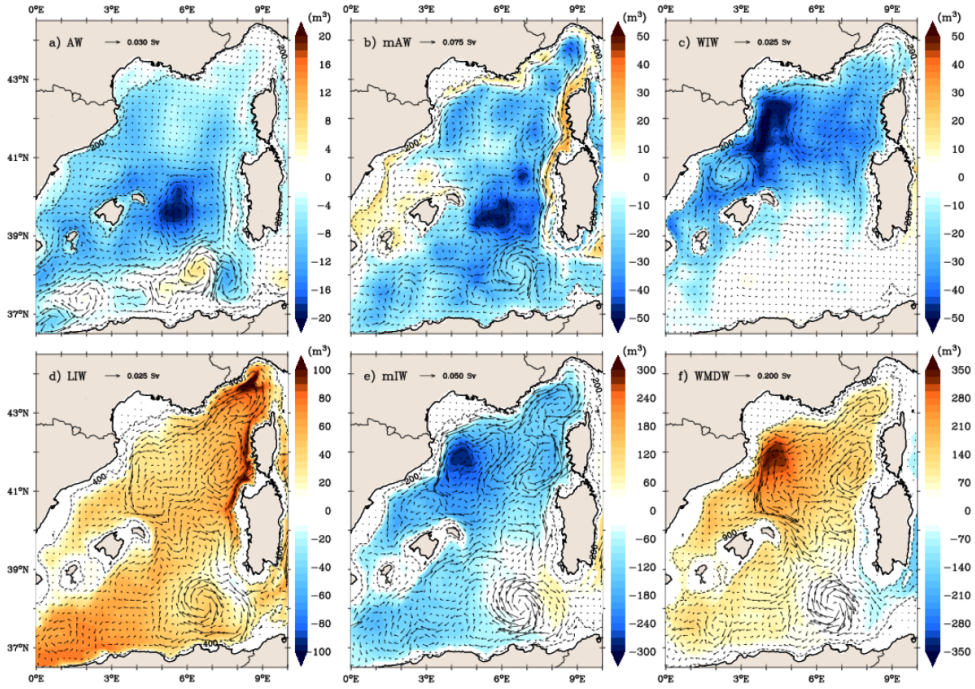

Fig. 9. Differences of water mass volumes and transports between the average of 10 years without DWF and the average of 6 years with DWF (i.e., DWF minus no DWF) for Atlantic Water (a), modified Atlantic Water (b), Western Intermediate Water (c), Levantine Intermediate Water (e), mixed Intermediate Water (e) and Western Mediterranean Deep Water (f). A scale arrow for transport values is shown on each panel.

The time series of AW transport shows that it is not modified in the Channel of Sardinia in comparison with the previous years (still stronger in winter than summer), but its spatial distribution is more strongly affected (Fig. 10a) leading to a significant redistribution of the amount of AW over the whole basin. This redistribution shows a smaller volume of AW over the Balearic Islands contrasting with an accumulation in the eastern Algerian sub-basin in several AEs. In addition, part of the AW is driven by the northward flow of mAW from the center of the Algerian basin into the WCC. This unusual AW spatial distribution is consistent with Barral et al. (2021) who reported an anomalous northward extension of the AW-mAW haline frontal zone in 2009, while DWF years are generally characterized by a southward migration of the haline front. The lower amount of AW around the Balearic Archipelago is clearly due to the increased influx of mAW in the Balearic Sea and the WIW anticyclonic structures, preventing the usual northward summer inflow of AW through the Balearic channels (e.g., Mason & Pascual, 2013; Vargas-Yanez et al., 2020).

The transports of LIW and mIW through the Sardinia Channel are also modified after this exceptional event, but at a lower level and with a 6-month delay. Again, the impact is more pronounced on their regional circulations throughout the basin. The positive anomaly of LIW volume over the entire Algero-Provençal basin is coherent with Fig. 9d as 2009 is a DWF year..

The greater amount in the Ligurian is likely due to the northward accumulation and entrainment by the mAW flow, while the negative LIW volume anomaly in the Sardinia Channel may reflect the thinning of the LIW layer due to the larger inflow of mAW and the larger outflow of WMDW. The amount of mIW decreases throughout the basin, first because of the winter DWF in the Provençal basin (as shown in Fig. 9e), and second because mIW is trapped between a shallower WMDW upper boundary and a deeper AW/mAW lower boundary, especially over the shelf slope of western Sardinia and Corsica (Fig. 3hkl).

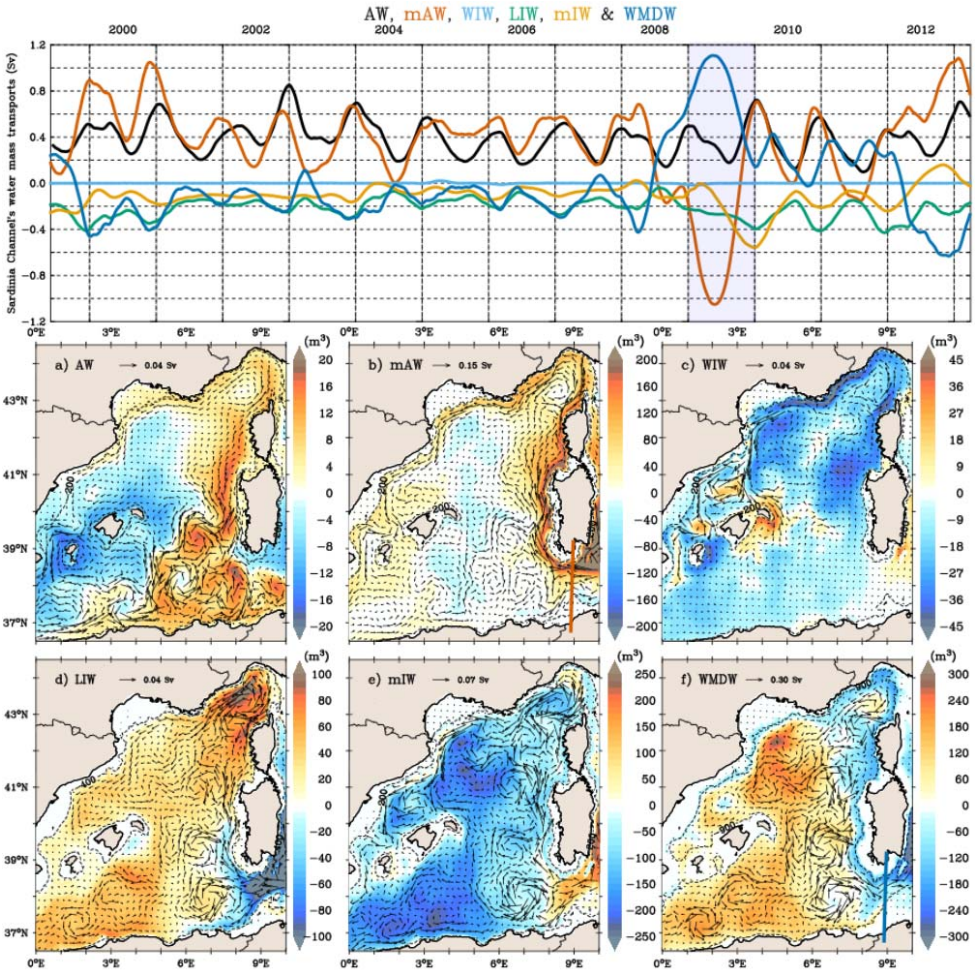

Fig. 10. Time series of water mass transport (Sv, positive eastward) through the Sardinian Channel (upper panel, water mass color codes shown at the top and volume and water mass transport anomalies in 2009 compared with the climatology of Fig. 8 (lower panels) for Atlantic waters (a), modified Atlantic waters (b), western intermediate waters (c), Levantine intermediate waters (e), mixed intermediate waters (e) and deep western Mediterranean waters (f). The section of the Strait of Sardinia is shown in panels b and f. Transport values in the upper panel are smoothed using a seasonal triangular filter.

4. Discussion and Conclusion

The main objective of this study was to extract from a 20-year reanalysis of the Western Mediterranean a coherent climatological picture of the water mass dynamics, focusing on the Algero-Provençal basin. To do this, we built a θ-S based algorithm that discriminates the main water masses in order to estimate the corresponding volumes and transports. Prior to the actual analysis, the calculated water mass mixing fractions were also used to estimate the mean thermohaline characteristics and depth range of each water mass. This allowed us to validate the behavior of the algorithm, i.e., to ensure that it could indeed report the correct water mass at the correct depth. Averaged over the 20 years of the reanalysis, the results give consistent distributions of the volumes and transports of the different water masses. The AW is mainly located in the AC and spread by the AEs over a large part of the Algerian basin. The mAW is produced in the area of AEs influence and flows cyclonically over most of the continental slopes of the basin. The WIW is produced in the Liguro-Provençal basin and the Gulf of Lion and accumulated in the Balearic Sea. The LIW is flowing and diluting towards the northwest, mainly by the SEs. The WMDW is produced by regular and realistic deep convection events in the Provençal area and flows southwards to accumulate in the deeper Algerian basin. The analysis of the time series of temperature, salinity and volumes brought several other positive elements, such as the coherent seasonally driven variability of AW, mAW and WIW, and the realistic inter-annual variability of WMDW production, particularly in 2005 which is known to be the major DWF event of the last three decades, given its impact on the intermediate and deep thermohaline characteristics (Schroeder et al., 2008ab).

This sudden exchange of mAW and WMDW between the Tyrrhenian and the Algero-Provençal basin leads to important changes in the regional distribution and circulation of surface and intermediate water masses over the whole western basin. The marked mAW influx from the Tyrrhenian induces a continuous flow along western Sardinia and Corsica that feeds the WCC and the NC as far as the Balearic Sea (Fig. 10b). The concomitant increase in mAW volume is likely responsible for the difference in mAW between years with and without DWF previously observed in Fig. 9b along western Sardinia and western Corsica, as well as the maximum peak in mAW volume over the entire basin in 2009 in Fig. 6d. Likewise, this arrival of warmer mAW from the Channel of Sardinia through the WCC leads to a negative anomaly in the WIW volume along the Liguro-Provençal continental slopes (Fig. 10c) whereas the lack in WIW around 42°N-5°E is consequent to the consumption of WIW by the 2009 DWF. The volume anomaly of WIW in the Balearic Sea shows increased escapes in the Ibiza Channel and northeast of Menorca, somewhat pushed by the mAW influx, but also the persistence of two distinct anticyclonic structures accumulating WIW in the central area and north of Ibiza. This latter has been reported

in Mason & Pascual (2013) as an anomalous SLA pattern in 2009, standing all year long but strengthened in Autumn.

Nevertheless, the times series also reveal spurious anomalies in the intermediate and deeper layers as mIW-WMDW coupled nonphysical variability in 1998-1999, 2003 and 2010 that have been assigned to assimilation biases. Those are due to subtle variations of salinity (0.02-0.04) slightly lowering (for the 2003 and 2010 cases) or hardly increasing (for the 1998-1999 case) potential density on a large part of the intermediate and deep waters. From this point, the somewhat fuzzy definition of the mIW may appear as the main shortcoming of our approach and should be discussed first. The mIW aggregates several water masses of diverse origins, such as TDW (which itself has diverse origins, e.g., Fuda et al., 2002; Buffet et al., 2017; Li & Tanhua, 2020; Iacono et al., 2021) and any waters possibly formed during intermediate or moderate convective events, and that do not fall into the typical WMDW category (such as the WDW in Bosse et al., 2016). The different intermediate water masses included in the mIW may have similar thermohaline characteristics and are distributed mainly along a LIW-WMDW mixing line. As such, they do not generate an inflection point on the θ-S diagram that could help to clearly discriminate them. Similarly, the algorithm does not distinguish Tyrrhenian Intermediate Water (TIW), a slightly warmer equivalent of the WIW formed in winter due to the Mistral channeled through the Strait of Bonifacio (Napolitano et al., 2019; Iacono et al., 2021). The TIW flows northward to the Corsican Channel and dilutes in the NC with average characteristics (θ~14°C, S~38.3 and σ_θ~28.8 kg m^{-3} in the reanalysis) similar to the mAW. The ideal way to properly sort TIW from the WIW-mAW set, and TDW from the mIW set, would be Lagrangian tracking of these water types along their trajectories from their original locations. This method has a development and computational cost that was quite prohibitive given the encouraging results we obtained with very early versions of the θ-S based algorithm (see Barral et al. 2020). Indeed, the presently defined mIW pool may be related to the finding of Millot (2013) as representative of all intermediate waters produced in areas of convection in the eastern basin, but extended here to the western basin as well. As so, it has an oceanographic sense, even if an oversimplified one, and it is not at the origin of the problem. Instead, its use helped to identify the three WMDW anomalous events.

Second, the regime shift suggested by the marked increase of the estimated LIW volume (briefly discussed in section 3.2) call for a discussion on the fact that the current algorithm does not take into account the warming and salinization trends observed throughout the Mediterranean in recent decades (e.g., Schroeder et al., 2017; Iona et al., 2018; Skliris et al., 2018; Vargas-Yanez et al., 2021; Fedele et al., 2022). Warming would not significantly affect water mass sorting when based on salinity ratio (i.e., for AW, mAW, and LIW), but would eventually lead WIW to be less marked and even disappearing, at least relative to their current definition. Juza et al. (2019) and Vargas-Yanez et al. (2021) showed a warming trend in WIW of 0.14-0.5°C over the last decade, but our results do not show a significant decrease in the amount of WIW over the 1993-2013 period. This can be explained by recalling that the current algorithm progressively marks WIW for a temperature below 13.5°C, whereas the usual temperature threshold used to identify it is 13°C. Preliminary tests using lower thresholds led to large underestimations of WIW volumes. The WIW temperature threshold was then set to keep the WIW volume estimates within the range of previous estimates and it appears, therefore, to implicitly parameterize the recent warming of the WIW. The most recent estimates of salinity trends in the Western Mediterranean range from 0.002 to 0.007 yr^{-1} depending on the area and period covered (Iona et al., 2018; Skliris et al., 2018; Vargas-Yanez et al., 2021; Fedele et al., 2022). Taking the most

extreme estimates, salinity changes over a 20-year period remain small (0.04-0.14) relative to the salinity ranges used by the algorithm to differentiate AW from mAW (2.35) and mAW from LIW (0.55). Furthermore, this trend appears to be more pronounced for AW than LIW (e.g., Vargas-Yanes, 2021; Fedele et al., 2022) so we do not expect serious bias in their fraction estimates. The problem is more questionable for the density-based water column partitioning, mainly for mIW-WMDW sorting which is very sensitive to small changes in potential density, as seen with the three anomalous events detected with the algorithm. Nevertheless, due to the nonlinear and antagonistic impact of salinity versus temperature changes on the sea state equation, the potential density trends observed for LIW or WMDW in the Western Mediterranean are small or insignificant (e.g., Vargas-Yanez et al., 2021) compared to the potential density values used in the algorithm to partition the water column. Therefore, we conclude that these warming and salinity trends would not have biased the estimated water mass fractions, and thus the subsequent volume and transport estimates. Nevertheless, it is clear that careful a priori consideration will be required for application on a longer time scale than the present 20 years analysis.

Validation or evaluation of a reanalysis is most often based on global statistics for heat and salt content, model misfit or assimilation increment, etc. (e.g., Hamon et al., 2016; Aznar et al., 2016). The approach we used goes further in this necessary assessment exercise as it allows us to identify at least three unrealistic events over the deep and intermediate layers that would be undetectable from global statistics given the small value of the salinity and temperature biases involved (fewer than 0.1, and than 0.3 °C). In fact, similar biases are likely to occur throughout the water column, but their impact would be much lower in the surface layers given the higher range of salinity and temperature variability between AW, mAW and WIW. Indeed, the removal of the three anomalous episodes shows no impact on surface volumes and circulations. This highlights a general weakness of contemporary reanalyses, which most often start in 1993 to benefit from the availability of altimetry data, but thus cover periods of very heterogeneous availability of in situ data. In the Mediterranean, the start of the ARGO era between 2000 and 2005 has led to a fivefold increase in available in situ profiles, but with still insufficient coverage of deep layers, especially for salinity (e.g., Hamon et al., 2016). Because deep salinity is the least constrained variable in assimilation systems, it is the most likely to suffer from assimilation bias. Nevertheless, we have shown that bypassing the biased periods allowed us to improve the average circulation scheme of the intermediate and deep water masses, mainly by retrieving the well known eastern Algerian barotropic Gyre (see Fig. 8def). This shows that the reanalysis is robust to accidental assimilation biases and we can expect deep-sea dynamics to be better constrained as more and more in situ deep-sea data become available for assimilation.

Beyond the assessment exercise, this study suggests new findings regarding the impact of the WMDW dynamics on surface and intermediate waters. The first is a possible breakdown of the eastern Algerian barotropic Gyre in response to the arrival of new WMDW in the southern part of the basin following significant DWF events occuring in the northern part. This disturbance of the Algerian Gyre has not been documented before from in situ data, but can be seen in Beuvier et al. (2012) who describes the southward propagation of WMDW cyclonic eddies after the strong DWF event of 2005 leading to a similar destabilization of the gyre in a model. Note that this deep gyre is not a true permanent feature in the reanalysis, but the average effect of the paths of several smaller (50-100 km) anticyclonic eddies. The velocities (and hence transports) in these eddies are about half the velocities of the southward spreading cyclonic eddies of the newly formed WMDW (about 5 cm s^{-1} vs 10 cm s^{-1}, Testor et al. 2005b; Beuvier et al., 2012). The

resulting eddy-eddy interactions are complex and chaotic (e.g., Waldman et al., 2018; Testor et al., 2018), so the disturbance of the deep gyre may simply reflect the mean of a more turbulent deep circulation. Of the sixteen years used to compute the two average regimes (i.e., after elimination of the four biased ones), six are DWF years while ten do not and DWF years occur more often at the end of the reanalysis, so that the two climatological regimes do not have the same statistical robustness. Nevertheless, the differences between the two regimes (DWF or no DWF) are coherent with the known acceleration of the northern cyclonic circulation of the surface (mAW), subsurface (WIW) and intermediate (LIW and mIW) layers (e.g., Madec et al., 1991; Herrmann et al., 2008), and with the southern shift of the AW/mAW main frontal zone suggested in Barral et al. (2021) during DWF years. The last issue concerns the deep water overflow in the Sardinia Channel following the 2009 DWF event, and its drastic impact on the circulations of intermediate and surface waters (Fig. 10). This overtopping is documented by Schroeder et al. (2016) as following the strong deep water renewal of 2005, the WMT, on which several other episodes accumulated from 2006 to 2010, bringing the upper boundary of deep water above the sill depth. The reanalysis appears to replicate this complex accumulation sequence over several years. The subsequent impact of the WMDW overflow on the AW, mAW, and WIW circulations seems globally coherent (discussed in more detail in Section 3.3), but the 2010 deep assimilation anomaly spoils the end of this sequence. Moreover, we did not find any independent estimate to validate the across strait eastward (westward) WMDW (mAW) transports (order 1 Sv) computed during the overflow event. Given the problems detected regarding the deep water dynamics in this reanalysis, more investigation will be needed to better corroborate these new findings regarding the impact of the DWF over surface and intermediate water mass dynamics throughout the Western Mediterranean. The way to do this are in progress by analyzing the satellite altimetry observations and, with the same algorithm of water mass sorting and derived proxies (volumes, transports), the twin free run of the MEDRYS1V2 reanalysis and another longer and finer reanalysis of the Mediterranean, precisely the CMEMS-MedRea reanalysis (1987-2019, 1/24°, Escudier et al., 2021). This should allow us to compare the impact of the detected assimilation biases, to get more robust climatological estimates and to enlarge the studied area to the Alboran and Tyrrhenian Seas.

Acknowledgements

This work was part of the PhD thesis of Q.-B. Barral funded by the French Ministère de l'Enseignement Supérieur, de la Recherche et de l'Innovation (MESRI). It is a contribution to the MISTRALS (Mediterranean INtegrated STudies at Regional And Local Scales) program through the CLOSCHEMED (CLOsure SCHEme of the MEDiterranean gyre) project funded by the French CNRS/INSU program LEFE-GMMC.

Appendix A : The detection algorithm of water masses in the Western Mediterranean.

First step of the algorithm, the partitioning of the water column involves the definitions of surface and deep layers. To locate the surface layer, two densities bound a linear function between the mAW (σ_{mAW}) and the LIW (σ_{LIW}). Above this σ_{mAW}, the surface flag is set to one while below σ_{LIW} , it is set to zero as :

968 $$flag_{surf} = \begin{cases} 1, \sigma < \sigma_{\mathrm{mAW}} \\ \frac{\sigma_{\mathrm{LIW}} - \sigma}{\sigma_{\mathrm{LIW}} - \sigma_{\mathrm{mAW}}}, \sigma_{\mathrm{mAW}} \leqslant \sigma \leqslant \sigma_{\mathrm{LIW}} \\ 0, \sigma > \sigma_{\mathrm{LIW}} \end{cases} \quad \text{(A.1)}$$

969 where σ_{mAW}=28.9643 kg m^{-3} (computed from S_{mAW}=38.45, θ_{mAW}=13.5°C) and σ_{LIW}=29.061 kg
970 m^{-3} (S_{LIW}=39, θ_{WMDW}=15°C), standing for the lower bound of the surface layer and the well
971 known core of the intermediate layer, respectively.

972 The separation of the deep layer of the water column from the intermediate is carried out in the
973 same way, but between the LIW and WMDW :

974 $$flag_{\mathrm{deep}} = \begin{cases} 0, \sigma < \sigma_{\mathrm{LIW}} \\ \frac{\sigma - \sigma_{\mathrm{LIW}}}{\sigma_{\mathrm{WMDW}} - \sigma_{\mathrm{LIW}}}, \sigma_{\mathrm{inf}} \leqslant \sigma \leqslant \sigma_{\mathrm{WMDW}} \\ 1, \sigma > \sigma_{\mathrm{WMDW}} \end{cases} \quad \text{(A.2)}$$

975 where σ_{LIW} remains as previously, and σ_{WMDW} = 29.1075 kg m^{-3} is computed from
976 S_{WMDW}=38.45, θ_{WMDW}=12.815°C.

977 The second step sorts the freshwater as a water with a salinity which is lower than the AW
978 salinity minimum (S_{AW}=36) :

979 $$flag_{fresh} = \begin{cases} \frac{S_{AW} - S}{S_{AW}}, S \leqslant S_{AW} \\ 0, S > S_{AW} \end{cases} \quad \text{(A.3)}$$

980 The flagging of AW hence uses a salinity ratio built to represent the AW-mAW mixing in the
981 surface layer :

982 $$flag_{\mathrm{AW}} = \begin{cases} (1 - flag_{\mathrm{fresh}}) \cdot flag_{\mathrm{surf}}, S < S_{\mathrm{AW}} \\ \left(\frac{S_{mAW} - S}{S_{mAW} - S_{AW}}\right) \cdot flag_{\mathrm{surf}}, S_{\mathrm{AW}} \leqslant S \leqslant S_{\mathrm{mAW}} \\ 0, S > S_{\mathrm{mAW}} \end{cases} \quad \text{(A.4)}$$

983 The LIW is defined assuming no salinity is higher than 39 in the western basin and that it dilutes
984 along a salinity gradient from 39 to 38.45 (the mAW salinity maximum) :

985 $$flag_{LIW} = \begin{cases} 0, S < S_{mAW} \\ \frac{S - S_{mAW}}{S_{LIW} - S_{mAW}}, S \geqslant S_{mAW} \end{cases} \quad \text{(A.5)}$$

986 The sum of previous water mass fractions defines a temporary flag that allows only the
987 remaining ratios to be treated :

988 $$tmp = flag_{fresh} + flag_{AW} + flag_{LIW} \quad \text{(A.6)}$$

989 Sorting the mAW and WIW assumes that they are pooled in the remaining surface waters and
990 can be discriminated using a temperature ratio :

991 $$flag_{WIW} = flag_{\mathrm{surf}} \cdot (1 - tmp) \cdot ratio_{WIW} \quad \text{(A.7a)}$$

992

993 $$flag_{mAW} = flag_{\mathrm{surf}} \cdot (1 - tmp) \cdot (1 - ratio_{\mathrm{WIW}}) \quad \text{(A.7b)}$$

994 where :

$$\sigma < \sigma_{\mathrm{LIW}} \Rightarrow ratio_{\mathrm{WIW}} = \begin{cases} 1, \theta < \theta_{\mathrm{WIW}} \\ \frac{\theta_{\mathrm{mAW}} - \theta}{\theta_{\mathrm{mAW}} - \theta_{\mathrm{WIW}}}, \theta_{\mathrm{WIW}} \leqslant \theta \leqslant \theta_{\mathrm{mAW}} \\ 0, \theta > \theta_{\mathrm{mAW}} \end{cases} \quad \text{(A.8)}$$

The last well-known water mass to define is WMDW which is simply located with the potential density ratio of (A.2) in the remaining waters of (A.6) :

$$flag_{WMDW} = (1 - tmp) \cdot flag_{\mathrm{deep}} \quad \text{(A.9)}$$

All known water masses being defined, mIW are defined as the rest of all flags :

$$flag_{mIW} = 1 - (flag_{fresh} + flag_{AW} + flag_{mAW} + flag_{WIW} + flag_{LIW} + flag_{WMDW}) \quad \text{(A.10)}$$

Appendix B : The characteristics, volumes and transports of the water masses.

The mean characteristics (θ, S, σ_θ and depth) of each water mass is computed as flag and volume weighted means, as for example for the mean potential temperature :

$$\overline{\theta_i}(t) = \frac{\sum_{xyz}(flag_i \cdot \Delta x \Delta y \Delta z \cdot \theta)}{\sum_{xyz}(flag_i \cdot \Delta x \Delta y \Delta z)} \quad \text{(B.1)}$$

where "i" is the water mass index (from 1 to 6 : AW, mAW, WIW, LIW, mIW, WMDW) and dx, dy and dz are the spatial increments defining the finite volume of one grid mesh. Note that the model grid being curvilinear and bottom adjusted for the deepest wet grid meshes (partial step discrete mesh), the grid meshes dimensions vary in space. Indexes of spatial increments have been omitted for simplification in this and the following equations (except when essential). The estimate for the core of a water mass is similarly computed but retaining only the value of the maximum fraction inside each vertical profile.

Starting for a simple water column (i.e., at a fixed longitude and latitude location), the water mass volume is computed as :

$$V_i(x, y, t) = \int_z flag_i \cdot dV = \sum_z flag_i(x, y, z, t) \cdot \Delta x \Delta y \Delta z \quad \text{(B.2)}$$

This first quantity allows us to construct daily maps of the volumes of the different water masses. Suming over the whole domain (or a subdomain like for the NWMed area) leads to the total volume of each water mass. As the local (x,y,z,t) sum of all the water mass flags is always one, it is straightforward to show that the summing over all water masses gives the constant water column volume that is only bathymetry dependent, neglecting the dynamic height (SSH) that is only about a tens of centimeters over the Western Mediterranean.

Using the same flags based distribution principle, each water mass transport (Sv) over a water column is computed as :

$$\overrightarrow{M_i}(t) = \iint \left(flag_i \cdot \vec{U}\right) ds \approx \vec{\imath} \sum_k (flag_i \cdot u_\theta \cdot \Delta x_\theta \Delta z_\theta) + \vec{\jmath} \sum_k (flag_i \cdot v_\theta \cdot \Delta y_\theta \Delta z_\theta) \quad \text{(B.3)}$$

where "u_θ" and "v_θ" stand for the velocity components interpolated at the scalar (temperature and salinity) grid points, according to the used curvilinear and Arakawa C mesh grid. Similarly, the across-section transports are computed as :

$$M_i^S(t) = \iint \left(flag_i \cdot \vec{U} \cdot \vec{n}\right) ds \approx \sum_{N_S} \sum_k [flag_i \cdot (u_S \cdot \Delta x_u \cdot \Delta z_u + v_S \cdot \Delta y_v \cdot \Delta z_v)] \quad \text{(B.4)}$$

where "S" is the chosen section and "N_S" stands for the total number of grid points along the

section. The velocities u_S and v_S and corresponding increments (dxu, dzu, dyv and dz) are the original Arakawa C grid (no interpolation) following the rules for sign and discretization as specified in the "cdftransport" routine of the Drakkar CDFTOOLS package (http://meom-group.github.io/code/). This grid specific computation was necessary to obtain a precise budget of the total transport when applied over all frontiers of a sub-region. As previously shown for the volumes, summing those transports on all water masses conserves the total transports, either on a water column, or a boundary section.

References

- Product/Dataset:

NOAA National Geophysical Data Center. 2009: ETOPO1 1 Arc-Minute Global Relief Model. NOAA National Centers for Environmental Information. https://www.ngdc.noaa.gov/mgg/global/ Accessed September 2021.

Amitai, Y., Ashkenazy, Y., & Gildor, H. (2021). The Effect of the Source of Deep Water in the Eastern Mediterranean on Western Mediterranean Intermediate and Deep Water. *Frontiers in Marine Science*, *7*. https://doi.org/10.3389/fmars.2020.615975

Astraldi, M., & Gasparini, G. P. (1994). The Seasonal Characteristics of the Circulation in the Tyrrhenian Sea. In *Seasonal and Interannual Variability of the Western Mediterranean Sea* (pp. 115–134). American Geophysical Union (AGU). https://doi.org/10.1029/CE046p0115

Aznar, R., Sotillo, M. G., Cailleau, S., Lorente, P., Levier, B., Amo-Baladrón, A., et al. (2016). Strengths and weaknesses of the CMEMS forecasted and reanalyzed solutions for the Iberia–Biscay–Ireland (IBI) waters. *Journal of Marine Systems*, *159*, 1–14. https://doi.org/10.1016/j.jmarsys.2016.02.007

Balmaseda, M. A., Hernandez, F., Storto, A., Palmer, M. D., Alves, O., Shi, L., et al. (2015). The Ocean Reanalyses Intercomparison Project (ORA-IP). *Journal of Operational Oceanography*, *8*(sup1), s80–s97. https://doi.org/10.1080/1755876X.2015.1022329

Barral, Q.-B., Zakardjian, B., Dumas, F., Garreau, P., & Beuvier, J. (2020). Analysis of specific water masses transports in the Western Mediterranean in the MEDRYS1V2 twenty-one-year reanalysis. https://doi.org/10.5194/egusphere-egu2020-21979

Barral, Q.-B., Zakardjian, B., Dumas, F., Garreau, P., Testor, P., & Beuvier, J. (2021). Characterization of fronts in the Western Mediterranean with a special focus on the North Balearic Front. *Progress in Oceanography*, *197*, 102636. https://doi.org/10.1016/j.pocean.2021.102636

Bauch, D., & Cherniavskaia, E. (2018). Water Mass Classification on a Highly Variable Arctic Shelf Region: Origin of Laptev Sea Water Masses and Implications for the Nutrient Budget. *Journal of Geophysical Research: Oceans*, *123*(3), 1896–1906. https://doi.org/10.1002/2017JC013524

Ben Ismail, S., Schroeder, K., Sammari, C., Gasparini, G. P., Borghini, M., & Aleya, L. (2014). Interannual variability of water mass properties in the Tunisia–Sicily Channel. *Journal of Marine Systems*, *135*, 14–28. https://doi.org/10.1016/j.jmarsys.2013.06.010

1071 Ben Ismail, S., Schroeder, K., Chiggiato, J., Sparnocchia, S., Borghini, M. (2021). Long term
1072 changes monitored in two Mediterranean Channels. in von Schuckmann et al., (2021)
1073 Copernicus Marine Service Ocean State Report, Issue 5, *Journal of Operational*
1074 *Oceanography*, 14:sup1, 1-185, https://doi.org/10.1080/1755876X.2021.1946240

1075 Bensoussan, N., Cebrian, E., Dominici, J.-M., Kersting D.-K., Kipson, S., Kizilkaya, Z., Ocaña,
1076 O., Peirache, M., Zuberer, F., Ledoux, J.-B., Linares, C., Zabala, M., Buongiorno Nardelli, B.,
1077 Pisano, A., & Garrabou, J. (2019). Using CMEMS and the Mediterranean Marine Protected
1078 Areas sentinel network to track ocean warming effects in coastal areas. in von Schuckmann et
1079 al., (2019) Copernicus Marine Service Ocean State Report, Issue 3, *Journal of Operational*
1080 *Oceanography*, 12:sup1, S1-S123, https://doi.org/10.1080/1755876X.2019.1633075

1081 Béranger, K., Mortier, L., Gasparini, G.-P., Gervasio, L., Astraldi, M., & Crépon, M. (2004). The
1082 dynamics of the Sicily Strait: a comprehensive study from observations and models. *Deep Sea*
1083 *Research Part II: Topical Studies in Oceanography*, *51*(4–5), 411–440.
1084 https://doi.org/10.1016/j.dsr2.2003.08.004

1085 Béranger, K., Mortier, L., & Crépon, M. (2005). Seasonal variability of water transport through
1086 the Straits of Gibraltar, Sicily and Corsica, derived from a high-resolution model of the
1087 Mediterranean circulation. *Progr. Oceanogr.*, *66*(2–4), 341–364.
1088 https://doi.org/10.1016/j.pocean.2004.07.013

1089 Bergamasco, A., & Malanotte-Rizzoli, P. (2010). The circulation of the Mediterranean Sea: a
1090 historical review of experimental investigations. *Advances in Oceanography and Limnology*,
1091 *1*(1), 11–28. https://doi.org/10.1080/19475721.2010.491656

1092 Bethoux, J. (1980). Mean water fluxes across sections in the mediterranean-sea, evaluated on the
1093 basis of water and salt budgets and of observed salinities. *Oceanologica Acta*, *3*(1), 79–88.

1094 Bethoux, J. P., & Gentili, B. (1999). Functioning of the Mediterranean Sea: past and present
1095 changes related to freshwater input and climate changes. *Journal of Marine Systems*, *20*(1–4),
1096 33–47. https://doi.org/10.1016/S0924-7963(98)00069-4

1097 Bethoux, J. P., Prieur, L., & Nyffeler, F. (1982). The Water Circulation in the North-Western
1098 Mediterranean Sea, its Relations with Wind and Atmospheric Pressure. In J. C. J. Nihoul
1099 (Ed.), *Elsevier Oceanography Series* (Vol. 34, pp. 129–142). Elsevier.
1100 https://doi.org/10.1016/S0422-9894(08)71240-6

1101 Bethoux, J. P., Gentili, B., Morin, P., Nicolas, E., Pierre, C., & Ruiz-Pino, D. (1999). The
1102 Mediterranean Sea: a miniature ocean for climatic and environmental studies and a key for the
1103 climatic functioning of the North Atlantic. *Progress in Oceanography*, *44*(1–3), 131–146.
1104 https://doi.org/10.1016/S0079-6611(99)00023-3

1105 Béthoux, J.-P., Gentili, B., & Tailliez, D. (1998). Warming and freshwater budget change in the
1106 Mediterranean since the 1940s, their possible relation to the greenhouse effect. *Geophysical*
1107 *Research Letters*, *25*(7), 1023–1026. https://doi.org/10.1029/98GL00724

1108 Beuvier, J., Béranger, K., Lebeaupin Brossier, C., Somot, S., Sevault, F., Drillet, Y., et al. (2012).
1109 Spreading of the Western Mediterranean Deep Water after winter 2005: Time scales and deep
1110 cyclone transport. *Journal of Geophysical Research: Oceans*, *117*(C7), n/a-n/a.
1111 https://doi.org/10.1029/2011JC007679

1112 Beuvier, J., Hamon, M., Greiner, E., Drévillon, M., & Lellouche, J. (2016). New Version of

MEDRYS, A Mediterranean Sea Reanalysis During 1992-2013, Rapp. Comm. Int. Mer Medit. Vol.41 p.123, Proceedings of the 41th CIESM Congress, Kiel, Germany, september 2016.

Borghini, M., Bryden, H., Schroeder, K., Sparnocchia, S., & Vetrano, A. (2014). The Mediterranean is becoming saltier. *Ocean Science*, *10*(4), 693–700. https://doi.org/10.5194/os-10-693-2014

Bosse, A., Testor, P., Mortier, L., Prieur, L., Taillandier, V., d'Ortenzio, F., & Coppola, L. (2015). Spreading of Levantine Intermediate Waters by submesoscale coherent vortices in the northwestern Mediterranean Sea as observed with gliders. *Journal of Geophysical Research: Oceans*, *120*(3), 1599–1622. https://doi.org/10.1002/2014JC010263

Bosse, A., Testor, P., Houpert, L., Damien, P., Prieur, L., Hayes, D., et al. (2016). Scales and dynamics of Submesoscale Coherent Vortices formed by deep convection in the northwestern Mediterranean Sea. *Journal of Geophysical Research: Oceans*, *121*(10), 7716–7742. https://doi.org/10.1002/2016JC012144

de Brauwere, A., Jacquet, S. H. M., De Ridder, F., Dehairs, F., Pintelon, R., Schoukens, J., & Baeyens, W. (2007). Water mass distributions in the Southern Ocean derived from a parametric analysis of mixing water masses. *Journal of Geophysical Research*, *112*(C2), C02021. https://doi.org/10.1029/2006JC003742

Bryden, H. L., Candela, J., & Kinder, T. H. (1994). Exchange through the Strait of Gibraltar. *Progress in Oceanography*, *33*(3), 201–248. https://doi.org/10.1016/0079-6611(94)90028-0

Buffett, G. G., Krahmann, G., Klaeschen, D., Schroeder, K., Sallarès, V., Papenberg, C., et al. (2017). Seismic Oceanography in the Tyrrhenian Sea: Thermohaline Staircases, Eddies, and Internal Waves. *Journal of Geophysical Research: Oceans*, *122*(11), 8503–8523. https://doi.org/10.1002/2017JC012726

Cabanes, C., Grouazel, A., Schuckmann, K. von, Hamon, M., Turpin, V., Coatanoan, C., et al. (2013). The CORA dataset: validation and diagnostics of in-situ ocean temperature and salinity measurements. *Ocean Science*, *9*(1), 1–18. https://doi.org/10.5194/os-9-1-2013

Cacho, I., Grimalt, J. O., Sierro, F. J., Shackleton, N., & Canals, M. (2000). Evidence for enhanced Mediterranean thermohaline circulation during rapid climatic coolings. *Earth and Planetary Science Letters*, *183*(3–4), 417–429. https://doi.org/10.1016/S0012-821X(00)00296-X

Cacho, I., Grimalt, J. O., Canals, M., Sbaffi, L., Shackleton, N. J., Schönfeld, J., & Zahn, R. (2001). Variability of the western Mediterranean Sea surface temperature during the last 25,000 years and its connection with the Northern Hemisphere climatic changes. *Paleoceanography*, *16*(1), 40–52. https://doi.org/10.1029/2000PA000502

Cardin, V., & Celio, M. (1997). Cluster analysis as a statistical method for identification of the water bodies present in the Gulf of Trieste (Northern Adriatic Sea), 17.

Cardin, V., Civitarese, G., Hainbucher, D., Bensi, M., & Rubino, A. (2015). Thermohaline properties in the Eastern Mediterranean in the last three decades: is the basin returning to the pre-EMT situation? *Ocean Science*, *11*(1), 53–66. https://doi.org/10.5194/os-11-53-2015

Carracedo, L. I., Gilcoto, M., Mercier, H., & Pérez, F. F. (2014). Seasonal dynamics in the Azores–Gibraltar Strait region: A climatologically-based study. *Progress in Oceanography*,

122, 116–130. https://doi.org/10.1016/j.pocean.2013.12.005

CIESM, 2001. Round table session on Mediterranean water mass acronyms. 36th CIESM Congress, Monte Carlo, 26 September 2001 http://ciesm.org/events/RT5-WaterMassAcronyms.pdf

CIESM, 2002. Tracking long-term hydrological change in the Mediterranean Sea. Workshop Series, n°16, http://www.ciesm.org/online/monographs/Monaco02.html

Colin, J., Déqué, M., Radu, R., & Somot, S. (2010). Sensitivity study of heavy precipitation in Limited Area Model climate simulations: influence of the size of the domain and the use of the spectral nudging technique. *Tellus A: Dynamic Meteorology and Oceanography*, *62*(5), 591–604. https://doi.org/10.1111/j.1600-0870.2010.00467.x

Cortina-Guerra, A., Gomez-Navarro, J. J., Martrat, B., Montávez, J. P., Incarbona, A., Grimalt, J. O., et al. (2021). Northern Hemisphere atmospheric pattern enhancing Eastern Mediterranean Transient-type events during the past 1000 years. *Climate of the Past*, *17*(4), 1523–1532. https://doi.org/10.5194/cp-17-1523-2021

Crépon, M., & Boukthir, M. (1987). Effect of deep water formation on the circulation of the Ligurian Sea. *Effect of Deep Water Formation on the Circulation of the Ligurian Sea*, *5*(1), 43–48.

Dee, D. P., Uppala, S. M., Simmons, A. J., Berrisford, P., Poli, P., Kobayashi, S., et al. (2011). The ERA-Interim reanalysis: configuration and performance of the data assimilation system. *Quarterly Journal of the Royal Meteorological Society*, *137*(656), 553–597. https://doi.org/10.1002/qj.828

Escudier, R., Mourre, B., Juza, M., & Tintoré, J. (2016). Subsurface circulation and mesoscale variability in the Algerian subbasin from altimeter-derived eddy trajectories. *Journal of Geophysical Research: Oceans*, *121*(8), 6310–6322. https://doi.org/10.1002/2016JC011760

Escudier, R., Clementi, E., Cipollone, A., Pistoia, J., Drudi, M., Grandi, A., et al. (2021). A High Resolution Reanalysis for the Mediterranean Sea. *Frontiers in Earth Science*, *9*, 1060. https://doi.org/10.3389/feart.2021.702285

Falco, P., Trani, M., & Zambianchi, E. (2016). Water mass structure and deep mixing processes in the Tyrrhenian Sea: Results from the VECTOR project. *Deep Sea Research Part I: Oceanographic Research Papers*, *113*, 7–21. https://doi.org/10.1016/j.dsr.2016.04.002

Fedele, G., Mauri, E., Notarstefano, G., & Poulain, P. M. (2022). Characterization of the Atlantic Water and Levantine Intermediate Water in the Mediterranean Sea using 20 years of Argo data. *Ocean Science*, *18*(1), 129–142. https://doi.org/10.5194/os-18-129-2022

Font, J., Puig, P., Salat, J., Palanques, A., & Emelianov, M. (2007). Sequence of hydrographic changes in NW Mediterranean deep water due to the exceptional winter of 2005. *Scientia Marina*, *71*(2), 339–346. https://doi.org/10.3989/scimar.2007.71n2339

Fox-Kemper, B., Adcroft, A., Böning, C. W., Chassignet, E. P., Curchitser, E., Danabasoglu, G., et al. (2019). Challenges and Prospects in Ocean Circulation Models. *Frontiers in Marine Science*, *0*. https://doi.org/10.3389/fmars.2019.00065

Fuda, J. L., Millot, C., Taupier-Letage, I., Send, U., & Bocognano, J. M. (2000). XBT monitoring of a meridian section across the western Mediterranean Sea. *Deep Sea Research Part I:*

Oceanographic Research Papers, *47*(11), 2191–2218. https://doi.org/10.1016/S0967-0637(00)00018-2

Fuda, J.-L., Etiope, G., Millot, C., Favali, P., Calcara, M., Smriglio, G., & Boschi, E. (2002). Warming, salting and origin of the Tyrrhenian Deep Water: Warming, salting and origin of the tyrrhenian deep water. *Geophysical Research Letters*, *29*(19), 4-1-4–4. https://doi.org/10.1029/2001GL014072

Gačić, M., Schroeder, K., Civitarese, G., Cosoli, S., Vetrano, A., & Eusebi Borzelli, G. L. (2013). Salinity in the Sicily Channel corroborates the role of the Adriatic–Ionian Bimodal Oscillating System (BiOS) in shaping the decadal variability of the Mediterranean overturning circulation. *Ocean Science*, *9*(1), 83–90. https://doi.org/10.5194/os-9-83-2013

Gao, Y., Huang, R. X., Zhu, J., Huang, Y., & Hu, J. (2020). Using the Sigma-Pi Diagram to Analyze Water Masses in the Northern South China Sea in Spring. *Journal of Geophysical Research: Oceans*, *125*(7), e2019JC015676. https://doi.org/10.1029/2019JC015676

García-Herrera, R., Díaz, J., Trigo, R. M., Luterbacher, J., & Fischer, E. M. (2010). A Review of the European Summer Heat Wave of 2003. *Critical Reviews in Environmental Science and Technology*, *40*(4), 267–306. https://doi.org/10.1080/10643380802238137

Gasparini, G. P., Ortona, A., Budillon, G., Astraldi, M., & Sansone, E. (2005). The effect of the Eastern Mediterranean Transient on the hydrographic characteristics in the Strait of Sicily and in the Tyrrhenian Sea. *Deep Sea Research Part I: Oceanographic Research Papers*, *52*(6), 915–935. https://doi.org/10.1016/j.dsr.2005.01.001

Hamon, M., Beuvier, J., Somot, S., Lellouche, J.-M., Greiner, E., Jordà, G., et al. (2016). Design and validation of MEDRYS, a Mediterranean Sea reanalysis over the period 1992–2013. *Ocean Science*, *12*(2), 577–599. https://doi.org/10.5194/os-12-577-2016

Hassoun, A. E. R., Guglielmi, V., Gemayel, E., Goyet, C., Saab, M. A.-A., Giani, M., et al. (2015). Is the Mediterranean Sea Circulation in a Steady State. *Journal of Water Resources and Ocean Science*, *4*(1), 6. https://doi.org/10.11648/j.wros.20150401.12

Herrmann, M., Estournel, C., Déqué, M., Marsaleix, P., Sevault, F., & Somot, S. (2008). Dense water formation in the Gulf of Lions shelf: Impact of atmospheric interannual variability and climate change. *Continental Shelf Research*, *28*(15), 2092–2112. https://doi.org/10.1016/j.csr.2008.03.003

Herrmann, M., Sevault, F., Beuvier, J., & Somot, S. (2010). What induced the exceptional 2005 convection event in the northwestern Mediterranean basin? Answers from a modeling study. *Journal of Geophysical Research: Oceans*, *115*(C12). https://doi.org/10.1029/2010JC006162

Hjelmervik, K. T., & Hjelmervik, K. (2013). Estimating temperature and salinity profiles using empirical orthogonal functions and clustering on historical measurements. *Ocean Dynamics*, *63*(7), 809–821. https://doi.org/10.1007/s10236-013-0623-3

Houpert, L., Durrieu de Madron, X., Testor, P., Bosse, A., D'Ortenzio, F., Bouin, M. N., et al. (2016). Observations of open-ocean deep convection in the northwestern Mediterranean Sea: Seasonal and interannual variability of mixing and deep water masses for the 2007-2013 Period. *Journal of Geophysical Research: Oceans*, *121*(11), 8139–8171. https://doi.org/10.1002/2016JC011857

Iacono, R., Napolitano, E., Palma, M., & Sannino, G. (2021). The Tyrrhenian Sea Circulation: A Review of Recent Work. *Sustainability*, *13*(11), 6371. https://doi.org/10.3390/su13116371

Incarbona, A., Martrat, B., Mortyn, P. G., Sprovieri, M., Ziveri, P., Gogou, A., et al. (2016). Mediterranean circulation perturbations over the last five centuries: Relevance to past Eastern Mediterranean Transient-type events. *Scientific Reports*, *6*(1), 29623. https://doi.org/10.1038/srep29623

Iona, A., Theodorou, A., Sofianos, S., Watelet, S., Troupin, C., & Beckers, J.-M. (2018). Mediterranean Sea climatic indices: monitoring long-term variability and climate changes. *Earth System Science Data*, *10*(4), 1829–1842. https://doi.org/10.5194/essd-10-1829-2018

Isern-Fontanet, J., García-Ladona, E., & Font, J. (2006). Vortices of the Mediterranean Sea: An Altimetric Perspective. *Journal of Physical Oceanography*, *36*(1), 87–103. https://doi.org/10.1175/JPO2826.1

Jebri, F., Birol, F., Zakardjian, B., Bouffard, J., & Sammari, C. (2016). Exploiting coastal altimetry to improve the surface circulation scheme over the central Mediterranean Sea. *Journal of Geophysical Research: Oceans*, *121*(7), 4888–4909. https://doi.org/10.1002/2016JC011961

Juza, M., Renault, L., Ruiz, S., & Tintoré, J. (2013). Origin and pathways of Winter Intermediate Water in the Northwestern Mediterranean Sea using observations and numerical simulation: Origin and Pathways of Wiw in Nwmed. *Journal of Geophysical Research: Oceans*, *118*(12), 6621–6633. https://doi.org/10.1002/2013JC009231

Juza, M., Mourre, B., Lellouche, J.-M., Tonani, M., & Tintoré, J. (2015). From basin to sub-basin scale assessment and intercomparison of numerical simulations in the Western Mediterranean Sea. *Journal of Marine Systems*, *149*, 36–49. https://doi.org/10.1016/j.jmarsys.2015.04.010

Juza, M., Escudier, R., Vargas-Yáñez, M., Mourre, B., Heslop, E., Allen, J., & Tintoré, J. (2019). Characterization of changes in Western Intermediate Water properties enabled by an innovative geometry-based detection approach. *Journal of Marine Systems*, *191*, 1–12. https://doi.org/10.1016/j.jmarsys.2018.11.003

Kim, K., Kim, K.-R., Rhee, T. S., Rho, H. K., Limeburner, R., & Beardsley, R. C. (1991). Identification of Water Masses in the Yellow Sea and the East China Sea by Cluster Analysis. In K. Takano (Ed.), *Elsevier Oceanography Series* (Vol. 54, pp. 253–267). Elsevier. https://doi.org/10.1016/S0422-9894(08)70100-4

Knoll, M., Borrione, I., Fiekas, H.-V., Funk, A., Hemming, M. P., Kaiser, J., et al. (2017). Hydrography and circulation west of Sardinia in June 2014. *Ocean Science*, *13*(6), 889–904. https://doi.org/10.5194/os-13-889-2017

Krahmann, G., & Schott, F. (1998). Longterm increases in western Mediterranean salinities and temperatures: Anthropogenic and climatic sources. *Geophysical Research Letters*, *25*(22), 4209–4212. https://doi.org/10.1029/1998GL900143

Kubin, E., Poulain, P.-M., Mauri, E., Menna, M., & Notarstefano, G. (2019). Levantine Intermediate and Levantine Deep Water Formation: An Argo Float Study from 2001 to 2017. *Water*, *11*(9), 1781. https://doi.org/10.3390/w11091781

Lellouche, J.-M., Le Galloudec, O., Drévillon, M., Régnier, C., Greiner, E., Garric, G., et al.

(2013). Evaluation of global monitoring and forecasting systems at Mercator Océan. *Ocean Science*, *9*(1), 57–81. https://doi.org/10.5194/os-9-57-2013

Li, P., & Tanhua, T. (2020). Recent Changes in Deep Ventilation of the Mediterranean Sea; Evidence From Long-Term Transient Tracer Observations. *Frontiers in Marine Science*, *7*, 594. https://doi.org/10.3389/fmars.2020.00594

López-Jurado, J.-L., González-Pola, C., & Vélez-Belchí, P. (2005). Observation of an abrupt disruption of the long-term warming trend at the Balearic Sea, western Mediterranean Sea, in summer 2005. *Geophysical Research Letters*, *32*(24). https://doi.org/10.1029/2005GL024430

Madec, G., Delecluse, P., Crepon, M., & Chartier, M. (1991). A Three-Dimensional Numerical Study of Deep-Water Formation in the Northwestern Mediterranean Sea. *Journal of Physical Oceanography*, *21*(9), 1349–1371. https://doi.org/10.1175/1520-0485(1991)021<1349:ATDNSO>2.0.CO;2

Mallil, K., Testor, P., Bosse, A., Margirier, F., Houpert, L., Le Goff, H., et al. (2021). The Levantine Intermediate Water in the western Mediterranean and its interactions with the Algerian Gyres: insights from 60 years of observation. *Ocean Science Discussions*, 1–26. https://doi.org/10.5194/os-2021-120

Manca, B. B., Ibello, V., Pacciaroni, M., Scarazzato, P., & Giorgetti, A. (2006). Ventilation of deep waters in the Adriatic and Ionian Seas following changes in thermohaline circulation of the Eastern Mediterranean. *Climate Research*, *31*(2–3), 239–256. https://doi.org/10.3354/cr031239

Manzella, G. M. R., & La Violette, P. E. (1990). The seasonal variation of water mass content in the western Mediterranean and its relationship with the inflows through the straits of Gibraltar and Sicily. *Journal of Geophysical Research*, *95*(C2), 1623. https://doi.org/10.1029/JC095iC02p01623

Mariotti, A., Struglia, M. V., & Zeng, N. (2002). The Hydrological Cycle in the Mediterranean Region and Implications for the Water Budget of the Mediterranean Sea. *Journal of Climate*, *15*, 17.

Marty, J. C., & Chiavérini, J. (2010). Hydrological changes in the Ligurian Sea (NW Mediterranean, DYFAMED site) during 1995–2007 and biogeochemical consequences. *Biogeosciences*, *7*(7), 2117–2128. https://doi.org/10.5194/bg-7-2117-2010

Mason, E., & Pascual, A. (2013). Multiscale variability in the Balearic Sea: An altimetric perspective: Balearic Sea Variability. *Journal of Geophysical Research: Oceans*, *118*(6), 3007–3025. https://doi.org/10.1002/jgrc.20234

MEDOC GROUP. (1970). Observation of Formation of Deep Water in the Mediterranean Sea, 1969. *Nature*, *227*(5262), 1037–1040. https://doi.org/10.1038/2271037a0

Millot, C. (1987). Circulation in the western mediterranean-sea. *Oceanologica Acta*, *10*(2), 143–149.

Millot, C. (1990). The Gulf of Lions' hydrodynamics. *Continental Shelf Research*, *10*(9–11), 885–894. https://doi.org/10.1016/0278-4343(90)90065-T

Millot, C. (1999). Circulation in the Western Mediterranean Sea. *Journal of Marine Systems*, *20*(1), 423–442. https://doi.org/10.1016/S0924-7963(98)00078-5

Millot, C. (2007). Interannual salinification of the Mediterranean inflow. *Geophysical Research Letters*, *34*(21). https://doi.org/10.1029/2007GL031179

Millot, C. (2009). Another description of the Mediterranean Sea outflow. *Progress in Oceanography*, *82*(2), 101–124. https://doi.org/10.1016/j.pocean.2009.04.016

Millot, C. (2013). Levantine Intermediate Water characteristics: an astounding general misunderstanding! *Scientia Marina*, *77*(2), 217–232. https://doi.org/10.3989/scimar.03518.13A

Millot, C., & Taupier-Letage, I. (2005). Circulation in the Mediterranean Sea. In A. Saliot (Ed.), *The Mediterranean Sea* (Vol. 5K, pp. 29–66). Berlin, Heidelberg: Springer Berlin Heidelberg. https://doi.org/10.1007/b107143

Millot, C., Candela, J., Fuda, J.-L., & Tber, Y. (2006). Large warming and salinification of the Mediterranean outflow due to changes in its composition. *Deep Sea Research Part I: Oceanographic Research Papers*, *53*(4), 656–666. https://doi.org/10.1016/j.dsr.2005.12.017

Napolitano, E., Iacono, R., Ciuffardi, T., Reseghetti, F., Poulain, P.-M., & Notarstefano, G. (2019). The Tyrrhenian Intermediate Water (TIW): Characterization and formation mechanisms. *Progress in Oceanography*, *170*, 53–68. https://doi.org/10.1016/j.pocean.2018.10.017

Nof, D. (1979). On man-induced variations in the circulation of the Mediterranean Sea. *Tellus*, *31*(6), 558–564. https://doi.org/10.1111/j.2153-3490.1979.tb00937.x

Nykjaer, L. (2009). Mediterranean Sea surface warming 1985–2006. *Climate Research*, *39*, 11–17. https://doi.org/10.3354/cr00794

Olita, A., Sorgente, R., Natale, S., Gaberšek, S., Ribotti, A., Bonanno, A., & Patti, B. (2007). Effects of the 2003 European heatwave on the Central Mediterranean Sea: surface fluxes and the dynamical response. *Ocean Science*, *3*(2), 273–289. https://doi.org/10.5194/os-3-273-2007

Onken, R., & Sellschopp, J. (2001). Water masses and circulation between the eastern Algerian Basin and the Strait of Sicily in October 1996. *Oceanologica Acta*, *24*(2), 151–166. https://doi.org/10.1016/S0399-1784(00)01135-X

Ozer, T., Gertman, I., Kress, N., Silverman, J., & Herut, B. (2017). Interannual thermohaline (1979–2014) and nutrient (2002–2014) dynamics in the Levantine surface and intermediate water masses, SE Mediterranean Sea. *Global and Planetary Change*, *151*, 60–67. https://doi.org/10.1016/j.gloplacha.2016.04.001

Parras-Berrocal, I., Vazquez, R., CabosNarvaez, W. D., Sein, D., Esteban, O. A., Mejías, M. B., & Izquierdo, A. (2021). *Will deep water formation collapse in the North Western Mediterranean Sea by the end of the 21st century?* (preprint). Earth and Space Science Open Archive. Retrieved from http://www.essoar.org/doi/10.1002/essoar.10507698.1

Peliz, A., Boutov, D., & Teles-Machado, A. (2013). The Alboran Sea mesoscale in a long term high resolution simulation: Statistical analysis. *Ocean Modelling*, *72*, 32–52. https://doi.org/10.1016/j.ocemod.2013.07.002

Pellet, V., Aires, F., Munier, S., Fernández Prieto, D., Jordá, G., Dorigo, W. A., et al. (2019). Integrating multiple satellite observations into a coherent dataset to monitor the full water cycle – application to the Mediterranean region. *Hydrology and Earth System Sciences*, *23*(1),

1359 465–491. https://doi.org/10.5194/hess-23-465-2019

1360 Pessini, F., Olita, A., Cotroneo, Y., & Perilli, A. (2018). Mesoscale eddies in the Algerian Basin:
1361 do they differ as a function of their formation site? *Ocean Science*, *14*(4), 669–688.
1362 https://doi.org/10.5194/os-14-669-2018

1363 Pinardi, N., Cessi, P., Borile, F., & Wolfe, C. L. P. (2019). The Mediterranean Sea Overturning
1364 Circulation. *Journal of Physical Oceanography*, *49*(7), 1699–1721.
1365 https://doi.org/10.1175/JPO-D-18-0254.1

1366 Piñeiro, S., González-Pola, C., Fernández-Díaz, J. M., & Balbin, R. (2019). Thermohaline
1367 Evolution of the Western Mediterranean Deep Waters Since 2005: Diffusive Stages and
1368 Interannual Renewal Injections. *Journal of Geophysical Research: Oceans*, *124*(12), 8747–
1369 8766. https://doi.org/10.1029/2019JC015094

1370 Piñeiro, S., González-Pola, C., Fernández-Díaz, J. M., Naveira-Garabato, A. C., Sánchez-Leal,
1371 R., Puig, P., et al. (2021). Persistent, Depth-Intensified Mixing During The Western
1372 Mediterranean Transition's Initial Stages. *Journal of Geophysical Research: Oceans*, *126*(2).
1373 https://doi.org/10.1029/2020JC016535

1374 Pinot, J.-M., Tintoré, J., & Gomis, D. (1995). Multivariate analysis of the surface circulation in
1375 the Balearic Sea. *Progress in Oceanography*, *36*(4), 343–376. https://doi.org/10.1016/0079-
1376 6611(96)00003-1

1377 Pisano, A., Marullo, S., Artale, V., Falcini, F., Yang, C., Leonelli, F. E., et al. (2020). New
1378 Evidence of Mediterranean Climate Change and Variability from Sea Surface Temperature
1379 Observations. *Remote Sensing*, *12*(1), 132. https://doi.org/10.3390/rs12010132

1380 Prieur, L., Lefevre, D., Gorsky, G., Bianchi, M., Andersen, V., & Gratton, Y. (2003). Frontal
1381 Processes enhance productivity of the Alboran Sea: a tentative first synthesis of the Almofront
1382 2 experiment results, 14063. Presented at the EGS - AGU - EUG Joint Assembly.

1383 Prieur, Louis, D'ortenzio, F., Taillandier, V., & Testor, P. (2020). Physical Oceanography of the
1384 Ligurian Sea. In C. Migon, P. Nival, & A. Sciandra (Eds.), *The Mediterranean Sea in the Era*
1385 *of Global Change 1* (1st ed., pp. 49–78). Wiley. https://doi.org/10.1002/9781119706960.ch3

1386 Puig, P., Madron, X. D. de, Salat, J., Schroeder, K., Martín, J., Karageorgis, A. P., et al. (2013).
1387 Thick bottom nepheloid layers in the western Mediterranean generated by deep dense shelf
1388 water cascading. *Progress in Oceanography*, *111*, 1–23.
1389 https://doi.org/10.1016/j.pocean.2012.10.003

1390 Puillat, I., Taupier-Letage, I., & Millot, C. (2002). Algerian Eddies lifetime can near 3 years.
1391 *Journal of Marine Systems*, *31*(4), 245–259. https://doi.org/10.1016/S0924-7963(01)00056-2

1392 Puillat, I., Sorgente, R., Ribotti, A., Natale, S., & Echevin, V. (2006). Westward branching of
1393 LIW induced by Algerian anticyclonic eddies close to the Sardinian slope. *Chemistry and*
1394 *Ecology*, *22*(sup1), S293–S305. https://doi.org/10.1080/02757540600670760

1395 Reynolds, R. W., Smith, T. M., Liu, C., Chelton, D. B., Casey, K. S., & Schlax, M. G. (2007).
1396 Daily High-Resolution-Blended Analyses for Sea Surface Temperature. *Journal of Climate*,
1397 *20*(22), 5473–5496. https://doi.org/10.1175/2007JCLI1824.1

1398 Rhein, M., Send, U., Klein, B., & Krahmann, G. (1999). Interbasin deep water exchange in the
1399 western Mediterranean. *Journal of Geophysical Research: Oceans*, *104*(C10), 23495–23508.

https://doi.org/10.1029/1999JC900162

Rio, M. H., Guinehut, S., & Larnicol, G. (2011). New CNES-CLS09 global mean dynamic topography computed from the combination of GRACE data, altimetry, and in situ measurements. *Journal of Geophysical Research: Oceans*, *116*(C7). https://doi.org/10.1029/2010JC006505

Rixen, M., Beckers, J.-M., Levitus, S., Antonov, J., Boyer, T., Maillard, C., et al. (2005). The Western Mediterranean Deep Water: A proxy for climate change. *Geophysical Research Letters*, *32*(12). https://doi.org/10.1029/2005GL022702

Robinson, A. R., & Golnaraghi, M. (1994). The Physical and Dynamical Oceanography of the Mediterranean Sea. In P. Malanotte-Rizzoli & A. R. Robinson (Eds.), *Ocean Processes in Climate Dynamics: Global and Mediterranean Examples* (pp. 255–306). Dordrecht: Springer Netherlands. https://doi.org/10.1007/978-94-011-0870-6_12

Roether, W., Manca, B. B., Klein, B., Bregant, D., Georgopoulos, D., Beitzel, V., et al. (1996). Recent Changes in Eastern Mediterranean Deep Waters. *Science*, *271*(5247), 333–335. https://doi.org/10.1126/science.271.5247.333

Roether, W., Klein, B., Manca, B. B., Theocharis, A., & Kioroglou, S. (2007). Transient Eastern Mediterranean deep waters in response to the massive dense-water output of the Aegean Sea in the 1990s. *Progress in Oceanography*, *74*(4), 540–571. https://doi.org/10.1016/j.pocean.2007.03.001

Salat, J., & Font, J. (1987). Water mass structure near and offshore the Catalan coast during the winters of 1982 and 1983. *Water Mass Structure near and Offshore the Catalan Coast during the Winters of 1982 and 1983*, *5*(1), 48–54.

Sammari, C., Millot, C., Taupier-Letage, I., Stefani, A., & Brahim, M. (1999). Hydrological characteristics in the Tunisia–Sardinia–Sicily area during spring 1995. *Deep Sea Research Part I: Oceanographic Research Papers*, *46*(10), 1671–1703. https://doi.org/10.1016/S0967-0637(99)00026-6

Schauer, U., & Losch, M. (2019). "Freshwater" in the Ocean is Not a Useful Parameter in Climate Research. *Journal of Physical Oceanography*, *49*(9), 2309–2321. https://doi.org/10.1175/JPO-D-19-0102.1

Schneider, A., Tanhua, T., Roether, W., & Steinfeldt, R. (2014). Changes in ventilation of the Mediterranean Sea during the past 25 year. *Ocean Science*, *10*(1), 1–16. https://doi.org/10.5194/os-10-1-2014

Schröder, K., Gasparini, G. P., Tangherlini, M., & Astraldi, M. (2006). Deep and intermediate water in the western Mediterranean under the influence of the Eastern Mediterranean Transient. *Geophysical Research Letters*, *33*(21), L21607. https://doi.org/10.1029/2006GL027121

Schroeder, K., Ribotti, A., Borghini, M., Sorgente, R., Perilli, A., & Gasparini, G. P. (2008). An extensive western Mediterranean deep water renewal between 2004 and 2006. *Geophysical Research Letters*, *35*(18). https://doi.org/10.1029/2008GL035146

Schroeder, K., Taillandier, V., Vetrano, A., & Gasparini, G. P. (2008). The circulation of the western Mediterranean Sea in spring 2005 as inferred from observations and from model

outputs. *Deep Sea Research Part I: Oceanographic Research Papers*, *55*(8), 947–965. https://doi.org/10.1016/j.dsr.2008.04.003

Schroeder, K., Josey, S. A., Herrmann, M., Grignon, L., Gasparini, G. P., & Bryden, H. L. (2010). Abrupt warming and salting of the Western Mediterranean Deep Water after 2005: Atmospheric forcings and lateral advection. *Journal of Geophysical Research*, *115*(C8), C08029. https://doi.org/10.1029/2009JC005749

Schroeder, K., Chiggiato, J., Bryden, H. L., Borghini, M., & Ben Ismail, S. (2016). Abrupt climate shift in the Western Mediterranean Sea. *Scientific Reports*, *6*(1), 23009. https://doi.org/10.1038/srep23009

Schroeder, K., Chiggiato, J., Josey, S. A., Borghini, M., Aracri, S., & Sparnocchia, S. (2017). Rapid response to climate change in a marginal sea. *Scientific Reports*, *7*(1), 4065. https://doi.org/10.1038/s41598-017-04455-5

Schroeder, Katrin, Cozzi, S., Belgacem, M., Borghini, M., Cantoni, C., Durante, S., et al. (2020). Along-Path Evolution of Biogeochemical and Carbonate System Properties in the Intermediate Water of the Western Mediterranean. *Frontiers in Marine Science*, *7*. https://doi.org/10.3389/fmars.2020.00375

Send, U., & Testor, P. (2017). Direct Observations Reveal the Deep Circulation of the Western Mediterranean Sea. *Journal of Geophysical Research: Oceans*, *122*(12), 10091–10098. https://doi.org/10.1002/2016JC012679

de Sherbinin, A. (2014). Climate change hotspots mapping: what have we learned? *Climatic Change*, *123*(1), 23–37. https://doi.org/10.1007/s10584-013-0900-7

Sisma-Ventura, G., Kress, N., Silverman, J., Gertner, Y., Ozer, T., Biton, E., et al. (2021). Post-eastern Mediterranean Transient Oxygen Decline in the Deep Waters of the Southeast Mediterranean Sea Supports Weakening of Ventilation Rates. *Frontiers in Marine Science*, *7*. https://doi.org/10.3389/fmars.2020.598686

Skliris, N., Zika, J. D., Herold, L., Josey, S. A., & Marsh, R. (2018). Mediterranean sea water budget long-term trend inferred from salinity observations. *Climate Dynamics*, *51*(7–8), 2857–2876. https://doi.org/10.1007/s00382-017-4053-7

Somot, S., Sevault, F., & Déqué, M. (2006). Transient climate change scenario simulation of the Mediterranean Sea for the twenty-first century using a high-resolution ocean circulation model. *Climate Dynamics*, *27*(7), 851–879. https://doi.org/10.1007/s00382-006-0167-z

Somot, S., Sevault, F., Déqué, M., & Crépon, M. (2008). 21st century climate change scenario for the Mediterranean using a coupled atmosphere–ocean regional climate model. *Global and Planetary Change*, *63*(2–3), 112–126. https://doi.org/10.1016/j.gloplacha.2007.10.003

Somot, Samuel, Jorda, G., Harzallah, A., & Darmaraki, S. (2016). Sub-chapter 1.2.3. The Mediterranean Sea in the future climate projections. In J.-P. Moatti & S. Thiébault (Eds.), *The Mediterranean region under climate change* (pp. 93–104). IRD Éditions. https://doi.org/10.4000/books.irdeditions.23100

Somot, Samuel, Houpert, L., Sevault, F., Testor, P., Bosse, A., Taupier-Letage, I., et al. (2018). Characterizing, modelling and understanding the climate variability of the deep water formation in the North-Western Mediterranean Sea. *Climate Dynamics*, *51*(3), 1179–1210.

https://doi.org/10.1007/s00382-016-3295-0

Soto-Navarro, J., Criado-Aldeanueva, F., García-Lafuente, J., & Sánchez-Román, A. (2010). Estimation of the Atlantic inflow through the Strait of Gibraltar from climatological and in situ data. *Journal of Geophysical Research*, *115*(C10), C10023. https://doi.org/10.1029/2010JC006302

Sparnocchia, S., Gasparini, G. P., Astraldi, M., Borghini, M., & Pistek, P. (1999). Dynamics and mixing of the Eastern Mediterranean outflow in the Tyrrhenian basin. *Journal of Marine Systems*, *20*(1–4), 301–317. https://doi.org/10.1016/S0924-7963(98)00088-8

Testor, P., & Gascard, J.-C. (2003). Large-Scale Spreading of Deep Waters in the Western Mediterranean Sea by Submesoscale Coherent Eddies. *Journal of Physical Oceanography*, *33*(1), 75–87. https://doi.org/10.1175/1520-0485(2003)033<0075:LSSODW>2.0.CO;2

Testor, P., Béranger, K., & Mortier, L. (2005). Modeling the deep eddy field in the southwestern Mediterranean: The life cycle of Sardinian eddies. *Geophysical Research Letters*, *32*(13). https://doi.org/10.1029/2004GL022283

Testor, P., Send, U., Gascard, J.-C., Millot, C., Taupier-Letage, I., & Béranger, K. (2005). The mean circulation of the southwestern Mediterranean Sea: Algerian Gyres. *Journal of Geophysical Research*, *110*(C11), C11017. https://doi.org/10.1029/2004JC002861

Testor, Pierre, Bosse, A., Houpert, L., Margirier, F., Mortier, L., Legoff, H., et al. (2018). Multiscale Observations of Deep Convection in the Northwestern Mediterranean Sea During Winter 2012-2013 Using Multiple Platforms. *Journal of Geophysical Research: Oceans*, *123*(3), 1745–1776. https://doi.org/10.1002/2016JC012671

Theocharis, A., Georgopoulos, D., Lascaratos, A., & Nittis, K. (1993). Water masses and circulation in the central region of the Eastern Mediterranean: Eastern Ionian, South Aegean and Northwest Levantine, 1986–1987. *Deep Sea Research Part II: Topical Studies in Oceanography*, *40*(6), 1121–1142. https://doi.org/10.1016/0967-0645(93)90064-T

Theocharis, Alexander. (2008). Do we expect significant changes in the Thermohaline Circulation in the Mediterranean in relation to the observed surface layers warming?, 5.

Vara, A. de la, del Sastre, P. G., Arsouze, T., Gallardo, C., & Gaertner, M. Á. (2019). Role of atmospheric resolution in the long-term seasonal variability of the Tyrrhenian Sea circulation from a set of ocean hindcast simulations (1997–2008). *Ocean Modelling*, *134*, 51–67. https://doi.org/10.1016/j.ocemod.2019.01.004

Vargas-Yáñez, M., Moya, F., García-Martínez, M. C., Tel, E., Zunino, P., Plaza, F., et al. (2010). Climate change in the Western Mediterranean Sea 1900–2008. *Journal of Marine Systems*, *82*(3), 171–176. https://doi.org/10.1016/j.jmarsys.2010.04.013

Vargas-Yáñez, M., Zunino, P., Schroeder, K., López-Jurado, J. L., Plaza, F., Serra, M., et al. (2012). Extreme Western Intermediate Water formation in winter 2010. *Journal of Marine Systems*, *105–108*, 52–59. https://doi.org/10.1016/j.jmarsys.2012.05.010

Vargas-Yáñez, Manuel, Jesús García, M., Salat, J., García-Martínez, M. C., Pascual, J., & Moya, F. (2008). Warming trends and decadal variability in the Western Mediterranean shelf. *Global and Planetary Change*, *63*(2–3), 177–184. https://doi.org/10.1016/j.gloplacha.2007.09.001

Vargas-Yáñez, Manuel, Juza, M., Balbín, R., Velez-Belchí, P., García-Martínez, M. C., Moya, F.,

& Hernández-Guerra, A. (2020). Climatological Hydrographic Properties and Water Mass Transports in the Balearic Channels From Repeated Observations Over 1996–2019. *Frontiers in Marine Science*, *7*, 568602. https://doi.org/10.3389/fmars.2020.568602

Vargas-Yáñez, Manuel, Juza, M., García-Martínez, M. C., Moya, F., Balbín, R., Ballesteros, E., et al. (2021). Long-Term Changes in the Water Mass Properties in the Balearic Channels Over the Period 1996–2019. *Frontiers in Marine Science*, *8*. https://doi.org/10.3389/fmars.2021.640535

Waldman, R., Somot, S., Herrmann, M., Testor, P., Estournel, C., Sevault, F., et al. (2016). Estimating dense water volume and its evolution for the year 2012-2013 in the Northwestern Mediterranean Sea: An observing system simulation experiment approach: Estimating dense water volume. *Journal of Geophysical Research: Oceans*, *121*(9), 6696–6716. https://doi.org/10.1002/2016JC011694

Waldman, R., Herrmann, M., Somot, S., Arsouze, T., Benshila, R., Bosse, A., et al. (2017). Impact of the Mesoscale Dynamics on Ocean Deep Convection: The 2012-2013 Case Study in the Northwestern Mediterranean Sea. *Journal of Geophysical Research: Oceans*, *122*(11), 8813–8840. https://doi.org/10.1002/2016JC012587

Waldman, R., Somot, S., Herrmann, M., Bosse, A., Caniaux, G., Estournel, C., et al. (2017). Modeling the intense 2012-2013 dense water formation event in the northwestern Mediterranean Sea: Evaluation with an ensemble simulation approach: Modeling the 2012-2013 DWF event. *Journal of Geophysical Research: Oceans*, *122*(2), 1297–1324. https://doi.org/10.1002/2016JC012437

Waldman, R., Somot, S., Herrmann, M., Sevault, F., & Isachsen, P. E. (2018). On the Chaotic Variability of Deep Convection in the Mediterranean Sea. *Geophysical Research Letters*, *45*(5), 2433–2443. https://doi.org/10.1002/2017GL076319

Waldman, R., Brüggemann, N., Bosse, A., Spall, M., Somot, S., & Sevault, F. (2018). Overturning the Mediterranean Thermohaline Circulation. *Geophysical Research Letters*, *45*(16), 8407–8415. https://doi.org/10.1029/2018GL078502

Wüst, G. (1961). On the vertical circulation of the Mediterranean Sea. *Journal of Geophysical Research (1896-1977)*, *66*(10), 3261–3271. https://doi.org/10.1029/JZ066i010p03261

Younes, W. A. N., Bensoussan, N., Romano, J.-C., Arlhac, D., & Lafont, M.-G. (2003). Seasonal and interannual variations (1996–2000) of the coastal waters east of the Rhone river mouth as indicated by the SORCOM series. *Oceanologica Acta*, *26*(4), 311–321. https://doi.org/10.1016/S0399-1784(03)00037-9

Zhu, J., Zheng, Q., Hu, J., Lin, H., Chen, D., Chen, Z., et al. (2019). Classification and 3-D distribution of upper layer water masses in the northern South China Sea. *Acta Oceanologica Sinica*, *38*(4), 126–135. https://doi.org/10.1007/s13131-019-1418-2

Zunino, P., Schroeder, K., Vargas-Yáñez, M., Gasparini, G. P., Coppola, L., García-Martínez, M. C., & Moya-Ruiz, F. (2012). Effects of the Western Mediterranean Transition on the resident water masses: Pure warming, pure freshening and pure heaving. *Journal of Marine Systems*, *96–97*, 15–23. https://doi.org/10.1016/j.jmarsys.2012.01.011